Neural Computing and Applications
https://doi.org/10.1007/s00521-022-07967-y

ORIGINAL ARTICLE

Interpretable tourism volume forecasting with multivariate time series under the impact of COVID-19

Binrong Wu[1] · Lin Wang[1] · Rui Tao[1] · Yu-Rong Zeng[2]

Received: 27 April 2022 / Accepted: 17 October 2022

Abstract
This study proposes a novel interpretable framework to forecast the daily tourism volume of Jiuzhaigou Valley, Huangshan Mountain, and Siguniang Mountain in China under the impact of COVID-19 by using multivariate time-series data, particularly historical tourism volume data, COVID-19 data, the Baidu index, and weather data. For the first time, epidemic-related search engine data is introduced for tourism demand forecasting. A new method named the composition leading search index–variational mode decomposition is proposed to process search engine data. Meanwhile, to overcome the problem of insufficient interpretability of existing tourism demand forecasting, a new model of DE-TFT interpretable tourism demand forecasting is proposed in this study, in which the hyperparameters of temporal fusion transformers (TFT) are optimized intelligently and efficiently based on the differential evolution algorithm. TFT is an attention-based deep learning model that combines high-performance forecasting with interpretable analysis of temporal dynamics, displaying excellent performance in forecasting research. The TFT model produces an interpretable tourism demand forecast output, including the importance ranking of different input variables and attention analysis at different time steps. Besides, the validity of the proposed forecasting framework is verified based on three cases. Interpretable experimental results show that the epidemic-related search engine data can well reflect the concerns of tourists about tourism during the COVID-19 epidemic.

Keywords Interpretable tourism demand forecasting · Variational mode decomposition · Deep learning · COVID-19

1 Introduction

The outbreak of COVID-19 has imposed a huge impact on social behavior, the economy, and the environment [1]. In particular, globally affected by the COVID-19 epidemic, many countries have imposed national blockades and containment measures, which inevitably reduced the willingness to travel and paralyzed travel-related industries, such as airlines, hotels, and restaurants [2, 3]. As of August 2022, China, New Zealand, and Denmark, among other countries, have controlled the number of deaths and infections. These countries have been relaxing state controls and lifting lockdown measures, allowing companies to gradually start operations as long as they comply with government health and safety guidelines and rules and impose appropriate social distancing measures [4]. The domestic tourism industries in countries immensely affected by the COVID-19 epidemic have since been greatly restored. Subsequently, investigating the changes in tourism demand in those countries can provide guidance and insights into the recovery of tourism.

Equipped with foresight toward the post-pandemic scenario, the accurate prediction of tourism demand appears to be an extreme initiative for the strategic planning of tourism destinations and tourism-related companies [5, 6]. However,

✉ Yu-Rong Zeng
zyrhbue@gmail.com; zyr@hbue.edu.cn

Binrong Wu
binronghust@foxmail.com

Lin Wang
wanglin982@gmail.com

Rui Tao
taoruihust@foxmail.com

[1] School of Management, Huazhong University of Science and Technology, Wuhan 430074, China

[2] Hubei University of Economics, Wuhan 430205, China

Published online: 04 November 2022

the recurrence of epidemics brought about by the uncertainty of COVID-19 has also caused major challenges to the tourism demand forecast. Finding suitable indicators to reflect the people's concerns about the epidemic is critical in accurately making travel forecasts.

Search engine data can reflect tourist behavior and intentions. Expectedly, many scholars have focused on forecasting tourism volume by using Internet big data [7, 8]. The existing studies often use travel-related search indexes, such as tour, shopping, recreation, traffic, lodging, and dining data. However, to the best of our knowledge, no research has attempted to analyze the effect of epidemic-related search indexes on tourism prediction during the COVID-19 epidemic. Unlike previous studies, this study can contribute to predicting tourism demand based on tourism-related search indexes and epidemic-related search indexes. In particular, with Baidu occupying a relatively large market share in China [9], Baidu Index is adopted in this study.

The use of search engine data may face the problem of multicollinearity and overfitting. To reduce the complexity of the tourism demand forecasting model, researchers have proposed the use of one or many representative indicators as explanatory variables [10]. Different approaches, including the generalized dynamic factor model, principal component analysis, and Hurst exponent (HE)–time difference correlation (TDC) method, have been proposed for the composite index [11]. The composite index can help to avoid the problems of multicollinearity and overfitting [12].

Moreover, as the search form and the diversity of search purposes are often limited, a large amount of noise signal interference exists in search engine data [13]. Therefore, before prediction, a denoising pre-processing of data should be conducted given improve prediction accuracy [14, 15]. By decomposing the original search engine data sequence into different components, the ones that contribute the most to improving the prediction accuracy can be identified. Therefore, in this study, we innovatively combine the advantages of using composite and decomposed search indexes.

In particular, this study offers an effective approach for simultaneously utilizing historical tourism volume data, daily increase in confirmed cases, weather data, tourism-related search engine data, and epidemic-related search engine data. In this manner, the daily tourism volume of Jiuzhaigou Valley, Huangshan Mountain, and Siguniang Mountain—the three popular tourist attractions in China—can be systematically forecasted.

Most of the existing tourism demand forecasting models are limited to the research on the selection and processing of input variables while ignoring the analysis and interpretation of the coupling relationship between influencing factors and tourism demand. Although high accuracy has been achieved in some studies which are based on deep learning models and predict tourism demand in accordance with Internet data, the experimental model cannot well explain how the deep learning model works. To be specific, the insufficient explanation has created some obstacles for tourism-related workers to accept this research information. In other words, how tourism demand forecasts exhibit persuasive interpretability remains to be further investigated. Therefore, given the limitations of existing research, the Temporal Fusion Transformers (TFT) are improved in this study, followed by the construction of a high-quality interpretable tourism demand prediction model.

The main contributions of the current research can be summarized as follows:

(a) This study proposes a comprehensive interpretable tourism forecasting framework for incorporating tourism attention, epidemic situation, and weather conditions during the COVID-19 epidemic. Multi-source data can provide a relatively strong theory and comprehensive overview for tourism volume forecasting. The validity of the proposed forecasting framework is verified using the aforementioned three actual cases.

(b) It is one of the first attempts to model an interpretable tourism demand forecast based on Temporal Fusion Transformers. The analysis of the importance of different influencing factors affecting tourism demand via the interpretability of TFT contributes to identifying important influencing factors in tourism demand forecasting, thereby providing decision-makers with persuasive tourism demand forecasting analysis and decision-making assistance. Besides, the DE-TFT tourism demand prediction model is designed, and the parameters of the TFT are optimized based on the differential evolution algorithm (DE) to improve the prediction accuracy and stability. All in all, this study complements existing academic research on the interpretability of input variables in tourism forecasting, providing novel ideas for tourism volume forecasting in the post-epidemic era.

(c) To our knowledge, the current research is the first to introduce epidemic-related search engine data for tourism demand forecasting. The experimental results show that epidemic-related search data play a greater role in forecasting tourism volume than daily newly confirmed cases. A good reason is that epidemic-related data can sufficiently reflect the concerns of tourists about tourism during the COVID-19 epidemic.

(d) This study proposes a new method named the composition leading search index (CLSI)–variational mode decomposition (VMD) to process search engine

data, which is also an attempt to contribute theoretical insights into big data processing and the tourism demand forecasting methodology. CLSI, a method for processing high-dimensional data, is used to incorporate tourism-related and epidemic-related search engine data. This method is commonly employed in the financial and economic fields, but it is seldom used in tourism forecasting. VMD is used to further decompose the composite search index, and then the relationship investigation method is used to select the optimal sub-modes of VMD.

The remainder of this study is presented as follows. Section 2 summarizes the relevant research. Section 3 introduces several modes of basic theory analyses and presents the proposed forecasting framework of this study. Section 4 discusses the experimental study and research findings. Section 5 concludes this study and provides implications for managers.

2 Literature review

Researchers have explored various methods to predict tourism demand, and they mainly include econometric, time series, and artificial intelligence (AI)-based models [16–22]. With the development of big data analysis and Internet technology, Internet big data (e.g., social media data and search engine data) have attracted the attention of many scholars [14]. In particular, search engine data have become increasingly popular given their unique advantages, such as high-frequency and real-time characteristics, and the potential sensitivity of capturing consumer behavior. This section briefly summarizes the research on the use of search engine data for tourism forecasting and reviews the research on tourism demand forecasting under the influence of the different epidemics.

2.1 Tourism demand forecasting with search engine data

Search engine data—those data that users enter into search engines (e.g., Baidu and Google)—have recently provided social science with a new data source and a basis for analysis of human behavior [8]. Tourists or consumers often search and collect information through the Internet before taking any action. This type of information search provides tourism decision-makers and scholars with an information basis for analyzing the decision-making process and future behavior of tourism consumers [23].

Many studies show that search engine data can significantly improve the performance of tourism demand forecasting [24]. Bangwayo-Skeete and Skeete [25] proposed a composite search method from Google for "hotels and flights" and combined autoregressive mixed data sampling models with collected data from Google Trends to explain the remarkable forecasting performance of tourist volume in Caribbean destinations. Yang et al. [26] emphasized that the appropriate selection of search engine data according to the usage rate of search engines for different regions can help to more accurately forecast tourism demand. For example, Baidu data are more conducive to forecasting China's domestic travel demand, whereas Google data are more suitable for forecasting China's international travel demand.

The choice of keywords in the search engine data also directly determines the performance of tourism demand forecasting [27]. The existing studies have mainly relied on tourism-related domain knowledge and search engine data under specific categories for keyword selection. Considering that the data of search engines are huge and contain a wealth of information, scholars should choose the most appropriate information through selection and composite methods as a means of distinguishing between uncertain and accurate predictions [28]. On this basis, Peng et al. [11] selected the most useful keywords in their study based on HE and TDC analyses. However, the introduction of several highly relevant search query indicators may bring challenges to tourism prediction models. Given reducing the dimensions of search engine data, Li et al. [29] used a generalized dynamic factor model, Li et al. [10] applied principle component analysis, and Law et al. [30] used a deep learning approach to create composite search indexes. Their experiments demonstrated the validity of using the composite search index.

In recent years, decomposition methods have been widely used in tourism forecasting because these methods can reduce the complexity of the overall forecast without the need for additional data, thereby improving the accuracy of the forecast. Li and Law [19] used the ensemble empirical mode decomposition method to decompose search engine data from Google Trends for tourism demand forecasting. Their study proposed a unique decomposition-based perspective for big data processing based on the decomposition of search engine data. Nevertheless, little research has combined the advantages of using the composite search index and decomposition methods. By using CLSI and VMD to process the search engine data, this study can more fully tap the value of search engine data for tourism demand forecasting compared with previous works.

2.2 Tourism demand forecasting during the different pandemics

During the COVID-19 pandemic, the mobility of the tourism industry is subject to sudden and extreme restrictions [31]. A pandemic usually causes tourists to change their

travel plans because they are concerned about possible risks [32, 33].

As for tourism literature, Table 1 shows the epidemics and their effects as cited. Choe, Wang, and Song [34] found that the Middle East Respiratory Syndrome (MERS) coronavirus had a statistically and negatively significant effect on the tourism volume of visitors to South Korea. Shi and Li [35] discussed the influence of MERS on South Korea's inbound tourists. Their results revealed that MERS had a significant adverse impact on tourism demand; however, for official and business tourism arrivals, its impact was minimal. Zeng, Carter, and Lacy [36] determined the significant negative impact of the Severe Acute Respiratory Syndrome (SARS) epidemic on China's tourism development. McAleer et al. [37] found that the short-term and long-term effects of SARS on the entry of international tourists from Asia were greater than avian flu because travelers were more concerned about SARS. Page, Song, and Wu [32] proposed the time-varying parameter model to assess the simultaneous impact of the swine flu pandemic and the global economic crisis on the United Kingdom's inbound tourists.

Although only a few countries have experience in handling pandemics, two experiences can be drawn from their recovery measures. Firstly, prior to the elimination of the epidemic, the number of tourists had started to increase, but the recovery rate was extremely slow. Secondly, once the outbreak of the epidemic was eventually controlled, several months were observed before the return to normal levels, and the rapid increase was to levels higher than that before the outbreak. However, unlike the previous epidemic, COVID-19 has infected almost all countries, triggering an unprecedented global crisis. Gössling, Scott, and Hall [38] suggested that the COVID-19 crisis affects the tourism industry more than other types of crises.

Investigating the performance of tourism data as an epidemic occurs is critical in helping decision-makers to design smart measures, responses, and restriction plans, especially since events similar to COVID-19 are unpredictable [39]. The COVID-19 epidemic is highly uncertain and affects the future behavior of tourism. When an unpredictable external shock occurs, more research needs to be pursued to support the decision-making. On this basis, scholars have attempted to study the predictors of tourism demand during COVID-19. Wickramasinghe and Ratnasiri [5] used travel data classified by region and time and Google search data to improve the accuracy of travel forecasts in Sri Lanka during the COVID-19 pandemic. Liu et al. [40] and Zhang et al. [13] proposed scenario-based judgmental forecasting to analyze the amount of tourism recovery after the COVID-19 epidemic, respectively.

Table 1 Summary of selected tourism forecasting studies during the different pandemics

References	Type of epidemic	Search data frequency	Predicted variable	Input variables	Forecasting model
Choe et al. [34]	MERS	Monthly	Tourism volume visiting South Korea	Historical tourism volume data	The time-series model
Shi and Li [35]	MERS	Quarterly	South Korea's inbound tourists from China	GDP, CPI, the international oil price, and dummy variables	The autoregressive distributed lag model
Zeng et al. [36]	SARS	Yearly	International and domestic tourist arrivals	–	–
McAleer et al. [37]	SARS and Avian Flu	Monthly	International tourist arrivals to Asia	The numbers of SARS or Avian Flu infections and deaths	Static line fixed-effect model and a different transformation dynamic model
Page et al. [32]	The Swine Flu pandemic	Quarterly	Overseas arrivals and expenditure in the United Kingdom	GDP, Consumer Price Indices (CPI), and exchange rates	The Time-Varying Parameter model
Wickramasinghe and Ratnasiri [5]	COVID-19	Monthly	International arrivals to Sri Lanka	Google Trends and dummy variables to represent structural breaks	SARIMA
Liu et al. [40]	COVID-19	Quarterly	The 20 destinations worldwide	Scenario-based judgmental forecasting	Judgmental forecast
Zhang et al. [13]	COVID-19	Quarterly	Tourism recovery in Hong Kong	Scenario-based judgmental forecasting	The scenario-based Delphi adjustment forecasting approach

MERS middle east respiratory syndrome coronavirus, *SARS* severe acute respiratory syndrome epidemic, *COVID-19* coronavirus disease 2019

However, as shown in Table 1, the existing research on tourism prediction during the COVID-19 epidemic remains to be insufficient. This study introduces the number of epidemic infections and related epidemic search engine data to forecast tourism volume. This research mainly focuses on the changes in the number of tourists in different scenic spots from the perspective of the possible recurrence of the epidemic in China. Meanwhile, different from previous studies, this study introduces an interpretable forecasting deep learning model for tourism demand forecasting for the first time, which can provide a comprehensive explanation for tourist demand forecasting based on multi-source heterogeneous data.

3 Methodology

An integrated forecasting framework was used to incorporate historical tourism volume data, COVID-19 data, search engine data, weather data, and temperature data for forecasting daily tourism volume (Fig. 1). The framework entailed three steps: (a) data retrieval, (b) data processing and variable calculation, (c) tourism volume forecasting, and the generation of interpretable results from the DE-TFT model. In the first step, five types of daily data were collected to forecast the tourism volume of Jiuzhaigou Valley, Huangshan Mountain, and Siguniang Mountain under the impact of COVID-19. In the second step, the search engine data were divided into two categories: tourism-related data and epidemic-related data. CLSI was employed to aggregate the two types of data, and then VMD was used for the decomposition. Thereafter, the relationship investigation method was conducted to select the appropriate sub-sequences. The relationship investigation consisted of the stationarity test, co-integration test, and Granger relationship determination. As Baidu occupies a relatively large market share in China, this study used it as the search engine [9]. Finally, the DE-TFT interpretable prediction model was established to test the effect of multi-source heterogeneous big data in improving tourism volume prediction, and the interpretability results are given. The interpretability of TFT is primarily embodied in the three aspects as follows: the importance ranking of past inputs, the importance ranking of future inputs, and the attention to different lag orders. The variable selection network of the TFT model provides insights into the past or future inputs which are most important to tourism volume forecasting. TFT can also suggest the importance order of different lag orders, which is conducive to identifying suitable lag orders for tourism demand forecasting and probing into the effect of long- and short-term lag orders on tourism demand forecasting.

3.1 Basic theory analysis

3.1.1 Composition leading search index

In the field of tourism forecasting using Internet search data, selecting a method for data pre-processing is crucial in achieving an accurate prediction performance. CLSI, an efficient data synthesis method for handling Internet search indexes, was proposed by Liu et al. [41]. Taking Jiuzhaigou as an example, Fig. 2 shows the detailed procedures of tourism-related CLSI. The procedures of CLSI can be described as follows:

Step 1: Keyword selection. Keywords are divided into two categories: tourism-related keywords and epidemic-related keywords.

a. The step of defining the tourism-related keywords is based on the psychological process of Chinese tourists planning to visit a certain scenic spot. Visitors will first collect relevant information on search engines when planning to travel to a certain attraction. Six major aspects of tourism, namely tour, shopping, recreation, traffic, lodging, and dining, are usually considered. These six categories can be used to generate the seed keywords. Thereafter, the seed keywords can be utilized to obtain the relevant and frequent keywords appearing on the search engine interface. This method allows for the collected keywords to cover all aspects of the tourists' concerns.
b. As for the epidemic-related keywords, the travelers' concerns about the epidemic have significantly affected tourism demand. Nonetheless, such travelers' concerns can be reflected in the relevant search engine data. Three major aspects of COVID-19, namely epidemic, virus, and vaccine, are considered the seed keywords.

Step 2: Time difference measurement. Firstly, all keywords are linearly scaled between 0.1 and 0.9. TDC is a popular technique for testing the leading, consistent or lagging relationship of a time series. The formula is given by

$$r_l = \frac{\sum_{t=1}^{n}(x_{t+l}-\bar{x})(y_t-\bar{y})}{\sqrt{\sum_{t=1}^{n}(x_{t+l}-\bar{x})^2}\sum_{t=1}^{n}(y_t-\bar{y})^2}, l = 0, \pm 1, \pm 2, \pm 3, \ldots, \pm L, \quad (1)$$

where r_l represents the coefficient of cross-correlation with l, in which l is the leading period; y_t denotes tourism volume at time t, and $\bar{y}$ is the mean of y_t; x_t denotes the Internet search index, and $\bar{x}$ is the mean of x_t; and r_l is the correlation coefficient of x ahead of y in the l phases.

For tourism volume forecasting, keywords should have leading characteristics to tourism volume, i.e., $l \geq 1$. In

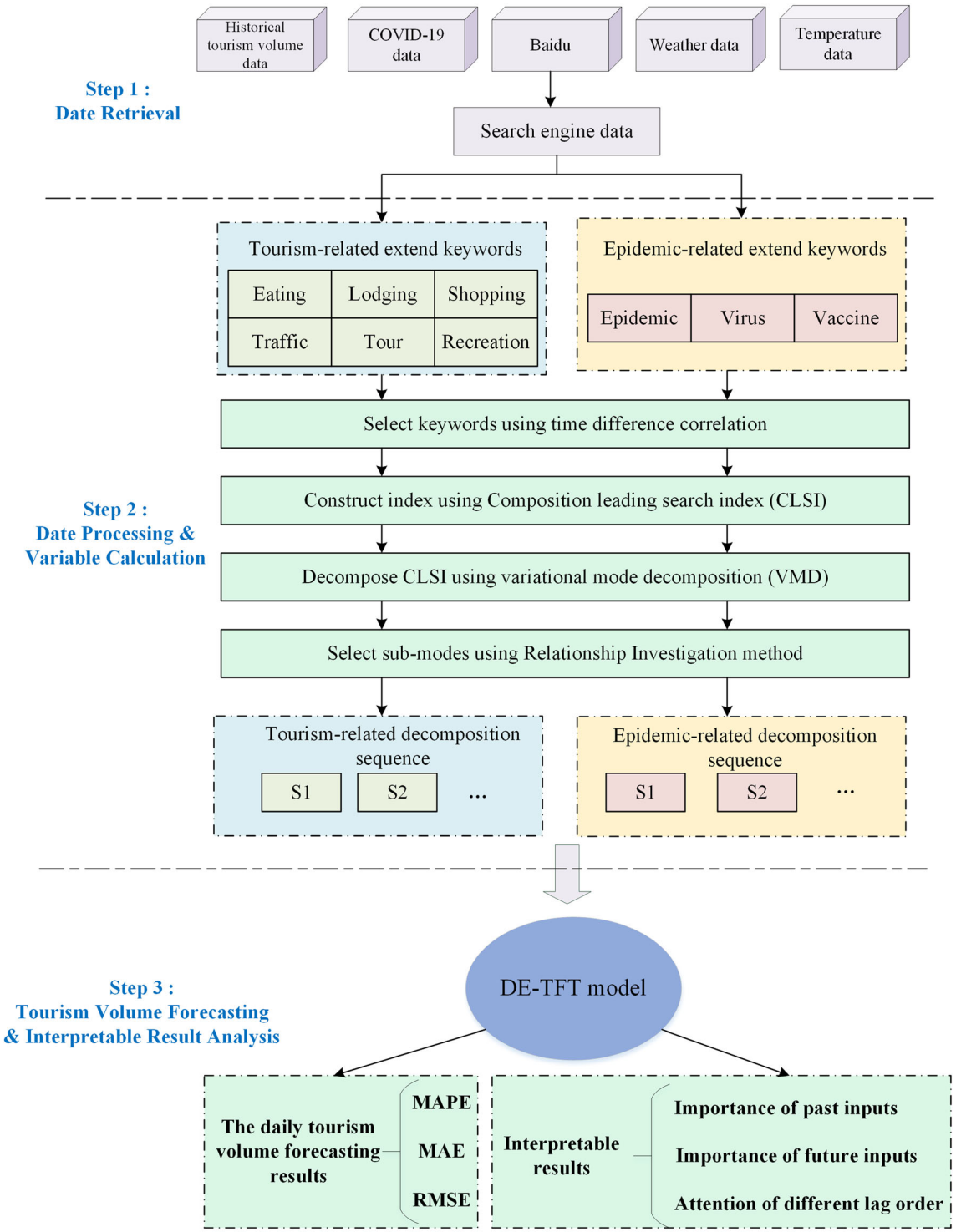

Fig. 1 Forecasting framework

particular, the leading characteristics indicate that the Baidu Index in the previous period exerts a guiding effect on the current tourism volume, that is, the Baidu Index contains predictive features for future tourism demand. TDC can identify whether the keywords maintain a leading characteristic to the tourism volume. Considering the timeliness of daily data, the maximum value of l was set to 3. Furthermore, the search value should contain the important factors affecting the tourism volume, and it should have low-noise characteristics to be able to handle

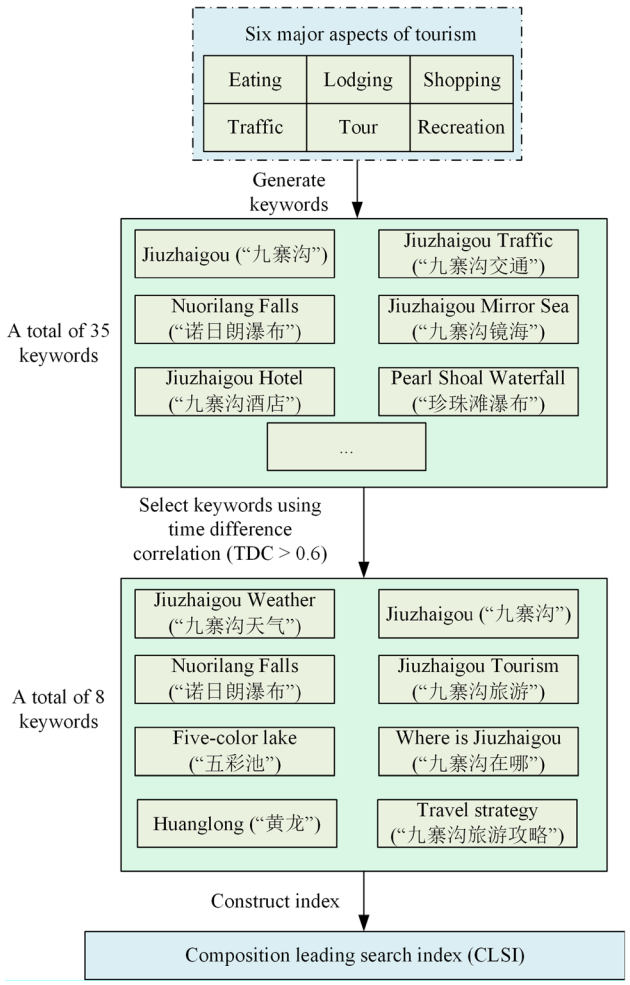

Fig. 2 The detailed procedures of tourism-related CLSI in Jiuzhaigou Valley

the tourism-related search engine data. The TDC threshold was set to 0.6. As for the epidemic-related search engine data, the TDC threshold was set to − 0.2. The keywords could then be filtered on the basis of $1 \le l \le 3$. The TDC was greater than 0.6 (for tourism-related data) or less than − 0.2 (for epidemic-related data).

Step 3: Leading index composition. As each keyword can only reflect one behavioral characteristic of tourists, the overall trend of tourism volume must be described using multiple keywords. The keywords selected in step 2 must be composited into a leading index. Given achieving this goal, TDC values were used to assign the weights of the different keywords. The greater the correlation between the keywords and tourism volume, the greater the weight, i.e., weight and correlation are linear. The sum of all search indexes constitutes the leading search index. The specific formula is given by:

$$\mathrm{CLSI}_t = \frac{\sum_{i=1}^{m} x_t * r_i}{m} \tag{2}$$

where m represents the total number of keywords, x_t denotes the Baidu Index at time t, r_i represents the maximum TDC value ($1 \le l \le 3$) between the tourism volume and Baidu Index corresponding to the ith keyword.

3.1.2 Variational mode decomposition

Dragomiretskiy and Zosso [42] proposed the use of VMD, an entirely non-recursive model. As a competitive signal decomposition method, VMD can be used to capture the irregular characteristics of the original data; furthermore, it has better adaptability and decomposition effects than empirical mode decomposition (EMD) [43]. In VMD, the origin signal $f(t)$ is decomposed by VMD to form multiple sub-modes (u_k, k=1, 2,…, K). Each sub-mode has a center frequency denoted by ω_k. The objective function of VMD is to minimize the sum of the frequency bandwidth of each sub-mode, and its constraint is the sum of each sub-mode being equal to the original signal. The formula is given by

$$\begin{aligned} &\underset{\{u_k\}\{\omega_k\}}{\text{minimum}} \left\{ \sum_{k=1}^{K} \partial_t \left\| \left[\left(\delta(t) + \frac{j}{\pi t} \right) * u_k(t) \right] e^{-j\omega_k t} \right\|_2^2 \right\} \\ &\text{s.t.} \sum_{k=1}^{K} u_k(t) = f(t), \end{aligned} \tag{3}$$

where $\delta(t)$ represents the Dirac distribution, and * denotes convolution. Thereafter, by introducing the quadratic penalty term alpha and the Lagrangian multiplier $\lambda(t)$, the constraint problem can be transformed into an unconstrained problem, allowing for the identification of the optimal solution to the abovementioned problem. The alpha can ensure that the sub-modes will be reconstructed accurately in the presence of Gaussian noise, while $\lambda(t)$ can ensure that the unconstrained problem will be equivalent to the constrained problem. The unconstrained problem can be described as follows:

$$\begin{aligned} &L(\{u_k\}, \{\omega_k\}, \lambda) \\ &= \text{alpha} \sum_{k=1}^{K} \left\| \partial_t \left[\left(\delta(t) + \frac{j}{\pi t} \right) * u_k(t) \right] e^{-j\omega_k t} \right\|_2^2 + \| f(t) \\ &- \sum_{k=1}^{K} u_k(t) \Big\|_2^2 + \left\langle \lambda(t), f(t) - \sum_{k=1}^{K} u_k(t) \right\rangle. \end{aligned} \tag{4}$$

The technique called the alternate direction method of multipliers (ADMM) can further solve the above problem. Iterating $u_k^{n+1}, \omega_k^{n+1}$ and λ^{n+1} obtains the saddle point of the

Lagrangian function. Then, $\widehat{u}_k^{n+1}$ and ω_k^{n+1} are updated by Eqs. (5) and (6), respectively. $\widehat{u}_k^{n+1}(\omega)$, $\widehat{u}_i(\omega)$, $\widehat{f}(\omega)$ and $\widehat{\lambda}(\omega)$ are the Fourier transform of $u_k^{n+1}(t)$, $u_i(t)$, $f(t)$ and $\lambda(t)$, respectively.

$$\widehat{u}_k^{n+1}(\omega) = \frac{\widehat{f}(\omega) - \sum_{i\neq k}\widehat{u}_i(\omega) + \frac{\widehat{\lambda}(\omega)}{2}}{1 + 2\text{alpha}(\omega - \omega_k)^2} \tag{5}$$

$$\omega_k^{n+1} = \frac{\int_0^\infty \omega|\widehat{u}_k(\omega)|^2 \mathrm{d}\omega}{\int_0^\infty |\widehat{u}_k(\omega)|^2 \mathrm{d}\omega} \tag{6}$$

According to ADMM, $\widehat{\lambda}^{n+1}(\omega)$ can be updated by Eq. (7), and τ denotes the updated parameter. The termination condition of the iteration is given by Eq. (8), in which ε denotes evaluation accuracy.

$$\widehat{\lambda}^{n+1}(\omega) = \widehat{\lambda}^{n}(\omega) + \tau(\widehat{f}(\omega) - \sum_{k=1}^{K}\widehat{u}_k^{n+1}(\omega) \tag{7}$$

$$\sum_{k=1}^{K}\frac{\|\widehat{u}_k^{n+1} - \widehat{u}_k^{n}\|_2^2}{\|\widehat{u}_k^{n}\|_2^2} < \varepsilon \tag{8}$$

Once the iteration ends, the real part of $\widehat{u}_k^{n+1}(\omega)$ can be converted into u_k^{n+1} by Fourier transform. That is, the final sub-modes are obtained by VMD.

Similar to the approach of Liu et al. [43], we used the ratio of residual energy r_{res} to determine the appropriate number of sub-modes. r_{res} is given by

$$r_{\text{res}} = \frac{1}{N_s}\sum_{t=1}^{N_s}\left|\frac{f(t) - \sum_{k=1}^{K}u_k(t)}{f(t)}\right|, \tag{9}$$

where $f(t)$ is the origin signal series; $u_k(t)$ is the decomposed sub-mode; K denotes the number of sub-modes; and N_s denotes the sample number. Empirically, when r_{res} has no obvious downward trend, the number of modes can be determined.

3.2 Forecasting models

3.2.1 Temporal Fusion transformers

With stronger interpretability than other black-box machine learning models, Temporal Fusion Transformers (TFT) is an interpretable multi-horizon time series prediction deep learning model proposed by the Google Cloud AI team [44]. The TFT model can characterize the relevant input features of three types of data (static input, past inputs, and known future inputs) efficiently, thereby providing high-performance solutions for various prediction problems.

The basic architecture of the TFT model consists of five parts: (a) Gating mechanism which functions to skip unused components; (b) Variable selection network which searches for relevant inputs at each time step via a variable selection network; (c) Static covariate encoder which integrates static features into the network and constraints temporal dynamics by encoding context vectors; (d) Temporal processing through which long- and short-term temporal relationships are learned from known variables; (e) Prediction intervals which are defined by quantiles forecast and determine the range of possible target values within each forecast interval. Specifically, the important modules of TFT employed in this study are introduced in detail as follows:

a. Gating mechanisms

Gated Residual Network (GRN) is applied to make the model flexible to mine the nonlinear relationship between variables and prediction targets. GRN contains two types of inputs, namely an optional external environment variable c and a primary input a. The mathematical expression of GRN is shown in Eqs. (10–12):

$$\text{GRN}_\omega(a, c) = \text{LayerNorm}(a + \text{GLU}_\omega(\eta_1)), \tag{10}$$

$$\eta_1 = W_{1,\omega}\eta_2 + b_{1,\omega}, \tag{11}$$

$$\eta_2 = \text{ELU}\left(W_{2,\omega}a + W_{3,\omega}c + b_{2,\omega}\right), \tag{12}$$

where η_1 and $\eta_2 \in \mathbb{R}^{d_{\text{model}}}$ denotes intermediate layers, LayerNorm represents the normalization of standard layers, ω denotes weight sharing, and ELU represents the Exponential Linear Unit activation function. Component gating layers based on Gated Linear Units (GLUs) provide certain flexibility to the TFT deep learning framework to skip any architectural parts that are not required for a given dataset. The mathematical description of GLUs is as follows:

$$\text{GLU}_\omega(\gamma) = \sigma\left(W_{4,\omega}\gamma + b_{4,\omega}\right) \odot \left(W_{5,\omega}\gamma + b_{5,\omega}\right), \tag{13}$$

where $\gamma \in \mathbb{R}^{d_{\text{model}}}$ denotes the input, $W_{(.)} \in \mathbb{R}^{d_{\text{model}}\times d_{\text{model}}}$ and $b_{(.)} \in \mathbb{R}^{d_{\text{model}}}$ denotes the weights and biases, $\sigma(.)$ means the element-wise Hadamard product, and d_{model} represents the size of the hidden state, and $\odot$ represents the element-wise Hadamard product. The GLU enables the TFT to control how much the GRN contributes to the original input. This layer can be skipped if desired, as the GLU output may be close to 0 to suppress the nonlinear contributions of the input variables.

b. Variable selection networks

The variable selection network provides insight into which variables are most important to the prediction problem. Let $[\text{I}]_t = \left[\xi_t^{(1)^\tau}, \ldots, \xi_t^{(m_x)^\tau}\right]^\tau$ denotes the flattened

vector of all past inputs. $\xi_t^{(j)}$ denotes the transformed input of the j th variable. In Eq. (14), the flat vector $[\mathrm{I}]_t$ and external environment variables c_s are fed into the GRN and then passed through a Softmax layer, resulting in variable selection weights V_{xt}. The explanatory properties of the TFT model are provided by variable selection weights. As shown in Eq. (15), each $\xi_t^{(j)}$ is nonlinearly processed by GRN. Thereafter, as shown in Eq. (16), the processed features are weighted and combined according to their variable selection weights, which $v_{xt}^{(j)}$ represents the jth element of the vector V_{xt}.

$$\mathrm{V}_{xt} = \mathrm{Softmax}\left(\mathrm{GRN}_{\mathrm{V}_x}\left([\mathrm{I}]_t, c_s\right)\right), \tag{14}$$

$$\widetilde{\xi}_t^{(j)} = \mathrm{GRN}_{\widetilde{\xi}(j)}\left(\xi_t^{(j)}\right), \tag{15}$$

$$\widetilde{\xi}_t = \sum_{j=1}^{m_x} v_{xt}^{(j)} \widetilde{\xi}_t^{(j)}, \tag{16}$$

iii. Interpretable multi-head attention

TFT modifies the multi-head attention structure of the underlying Transformer to enhance the interpretability of the model, thereby better learning the long-term relationship between different time steps. The self-attention mechanism contains three important elements, namely " queries $\mathrm{Q} \in \mathbb{R}^{N \times d_{attn}}$", " keys $\mathrm{K} \in \mathbb{R}^{N \times d_{attn}}$", and "value $\mathrm{V} \in \mathbb{R}^{N \times d_V}$". N represents the number of time steps from the input to the attention layer. The mathematical relationship between the three can be expressed by the following formula:

$$\mathrm{Attention}(Q, K, V) = A(Q, K)V, \tag{17}$$

$A()$ represents a normalization function. For attention values, a scaled dot product is usually used:

$$A(Q, K) = \mathrm{Softmax}\left(\frac{QK^T}{\sqrt{d_{attn}}}\right), \tag{18}$$

For the learning ability of the attention mechanism, multi-head attention is used to use different attention heads for different subspaces:

$$\mathrm{MultiHead}(Q, K, V) = [H_1, \ldots, H_{m_H}]W_H, \tag{19}$$

$$H_h = \mathrm{Attention}\left(QW_Q^{(h)}, KW_K^{(h)}, VW_V^{(h)}\right), \tag{20}$$

where $W_Q^{(h)} \in \mathbb{R}^{d_{\mathrm{model}} \times d_{attn}}$, $W_K^{(h)} \in \mathbb{R}^{d_{\mathrm{model}} \times d_{attn}}$ and $W_V^{(h)} \in \mathbb{R}^{d_{\mathrm{model}} \times d_v}$ represent weights of "queries", "keys", and "values" for specific headers, respectively. $W_H \in \mathbb{R}^{(m_H \cdot d_V) \times d_{\mathrm{model}}}$ denotes linearly connecting all attention heads H_h.

Considering that each attention head uses different values, attention weights alone cannot indicate the importance of specific features. Therefore, the multi-head attention is modified to a shared value in each attention head and aggregated using the addition of all heads, the mathematical expression is shown in Eq. (21–24):

$$\mathrm{InterpretableMultiHead}(Q, K, V) = \widetilde{H}W_H, \tag{21}$$

$$\widetilde{H} = \widetilde{A}(Q, K)VW_V, \tag{22}$$

$$= \left\{\frac{1}{m_H}\sum_{h=1}^{m_H} A(QW_Q^{(h)}, KW_K^{(h)})\right\}VW_V, \tag{23}$$

$$= \left\{\frac{1}{m_H}\sum_{h=1}^{m_H} \mathrm{Attention}(QW_Q^{(h)}, KW_K^{(h)}, VW_V)\right\}, \tag{24}$$

where $W_H \in \mathbb{R}^{d_{attn} \times d_{\mathrm{model}}}$ denotes that the final linear map is used, and $W_V \in \mathbb{R}^{d_{\mathrm{model}} \times d_V}$ represents a weight value shared by all attention heads.

iv. Quantile outputs and loss functions

TFT generates prediction intervals based on point predictions and does so by simultaneously predicting different percentiles (e.g., 10%, 50%, and 90%) at each time step. The quantile predictions are generated using a linear transformation of the temporal fusion decoder output, and the TFT is trained using a joint minimization of the quantile loss, summing the outputs of all quantiles, mathematically expressed as:

$$\mathcal{L}(\Omega, \mathrm{W}) = \sum_{y_t \in \Omega}\sum_{q \in \varrho}\sum_{T=1}^{T_{\max}} \frac{QL(y_t, \hat{y}(q, t-T, T), q)}{MT_{\max}}, \tag{25}$$

$$\mathrm{QL}(\mathrm{y}, \hat{y}, \mathrm{q}) = q(y - \hat{y})_+ + (1-q)(\hat{y} - y)_+, \tag{26}$$

where y denotes the actual values, $\hat{y}$ denotes the predicted values, Ω represents the domain of the training set containing M samples, ϱ represents the set of quantile inputs, W means the weights of the TFT model, and $(.)_+$ denotes $\max(0, .)$.

3.2.2 The proposed DE-TFT model

Figure 3 shows the basic architecture of the DE-TFT model. The key parameters of TFT include the number of batch sizes, number of time steps, number of hidden layers, number of attention heads, learning rates, and number of consecutive hidden layers, which have a great impact on the performance of TFT. However, in specific applications, it is difficult to set appropriate parameter values for these parameters. Therefore, this study uses the evolution

algorithm (DE) to intelligently and efficiently find the optimal values of the six key parameters of the TFT deep learning framework, in which MAPE is selected as the fitness function of DE. The basic steps of DE are described as follows.

Algorithm 1: DE algorithm

Begin
Input: Population: M; Dimension: D; Generation: T
Output: The best vector (solution) - Δ
For i = 1 to M **do**
  For j = 1 to D **do**
    $x_{i,t}^{j} = x_{min}^{j} + rand(0,1) \cdot (x_{max}^{j} - x_{min}^{j})$;
  end
end
While $(|f(\Delta)| \geq \varepsilon)$ or $t \leq T$ **do**
  For i = 1 to M **do**
    For j = 1 to D **do**
      $V_{i,t}^{j} = x_{i,t}^{j} + F * (x_{r1,t}^{j} - x_{r2,t}^{j})$ *//mutation, F is scaling factor, ranging in [0,2]. $x_{r1,t}^{j}$ and $x_{r2,t}^{j}$ are randomly selected individuals.*
      $u_{i,t}^{j} = \begin{cases} V_{i,t}^{j}, if\ rand(j) \leq CR\ or\ j = randn(t) \\ x_{i,t}^{j}, otherwise \end{cases}$ *//crossover, CR is distributed at interval [0, 1].*
    End
    If $f(u_{i,t}) < f(x_{i,t})$ **then**
      $x_{i,t} \leftarrow u_{i,t}$
      If $f(u_{i,t}) < f(\Delta)$ **then**
        $\Delta \leftarrow u_{i,t}$
      end
    else
      $x_{i,t} \leftarrow x_{i,t}$
    end
  end
  $t \leftarrow t + 1$
End
Return the best vector Δ

Historical tourism volume data, increased confirmed case data, and epidemic-related and tourism-related search engine data are input as past variables into DE-TFT, and at the same time, due to the existence of weather forecasts, weather data can be input into DE-TFT as known future variables. The predictive performance and interpretable results of the DE-TFT model are analyzed, and the predictive results are evaluated using MAPE, RMSE, and MAE.

The interpretable results are divided into three parts: the order of importance of past input variables, the order of importance of known future variables, and the attention of different lag orders. This study complements existing academic research on the interpretability of input variables in tourism forecasting and provides new ideas for tourism volume forecasting in the post-epidemic era.

3.2.3 Comparable models and evaluation metrics

This study uses five common forecasting models as comparable models to forecast tourism volume: the support vector machine (SVM), backpropagation neural network (BPNN), gated recurrent unit (GRU), and recurrent neural network (RNN), and long short-term memory (LSTM). The SVM, BPNN, GRU, RNN, and LSTM models have been widely used in the past and are known for achieving good performance in forecasting empirical studies [45–50]. For a fair comparison, the model specifications of these forecasting models are both selected by the DE algorithm.

The forecasting performances are generally evaluated based on a percentage error and two scale-dependent errors. The mathematical equations for calculating MAPE, RMSE, and MAE are given by

$$\text{MAPE} = \frac{\sum_{t=1}^{k} |\hat{y}_t - y_t|/y_t}{k}, \tag{27}$$

$$\text{RMSE} = \sqrt{\frac{\sum_{t=1}^{k} (\hat{y}_t - y_t)^2}{k}}, \tag{28}$$

$$\text{MAE} = \frac{1}{k} \sum_{t=1}^{k} |(\hat{y}_t - y_t)|, \tag{29}$$

where k denotes the size of forecasts; y_t represents the actual number of tourism arrivals at day t; and $\hat{y}_t$ represents the predicted number of tourism arrivals at day t.

4 Experimental study

The experimental study used Python 3.8 to implement DE-TFT and other comparable models. All deep learning models were trained on the CPU. The computation was evaluated on a personal computer with an *Intel (R) Core (TM) i7-10700 K CPU, 3.80 GHz, 32 GB RAM, and Windows 10 system.*

4.1 Data retrieval and pre-processing

Jiuzhaigou Valley, Huangshan Mountain, and Siguniang Mountain are among the most visited tourist destinations in China. Thus, this study selected these three scenic spots as the research objects. The collection and pre-processing of the relevant data (i.e., historical tourism volume data, epidemic data during COVID-19, search engine data, and weather data) for Jiuzhaigou Valley, Huangshan Mountain, and Siguniang Mountain tourism volume forecasting are given as follows.

(1) Historical tourism volume data

The daily tourism volume of each area was taken from their respective official websites. The details are shown in Fig. 4. For Jiuzhaigou Valley, the daily tourist arrival from April 1, 2020, to September 12, 2021, totals 530 observations. For Huangshan Mountain, the daily tourist arrival from March 1, 2020, to August 20, 2021 totals 538 observations. For Siguniang Mountain, the daily tourist arrival from April 1, 2020, to January 14, 2021 totals 289 observations.

(2) Epidemic data during the COVID-19 period

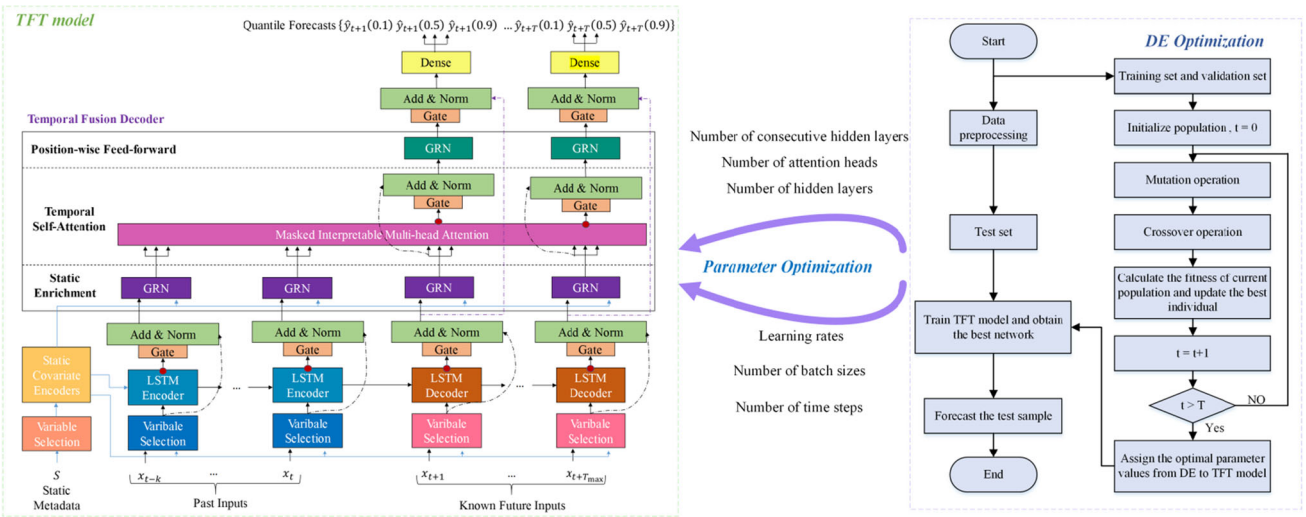

Fig. 3 The model architecture of the proposed DE-TFT model

In the post-epidemic era, the recurrence of epidemics in some areas affects the tourists' concerns. Thus, the impact of the epidemic data on the number of tourists was also considered in this study. The daily increase in the number of COVID-19 confirmed cases in China was collected from the National Health Commission of the People's Republic of China (http://www.nhc.gov.cn/) to forecast the tourism demand. To display the comparison in fluctuation between the increased number of confirmed cases and tourism volume in the three tourist attractions, the values are linearly scaled to be between 0.1 and 0.9 in this study. As shown in Fig. 5, the increase in the confirmed cases has significantly affected the tourism demand. Most especially, a wave of epidemics that began in July 2021 caused a rapid decline in tourist arrivals in scenic areas. However, after the epidemic was controlled at the end of August 2021, the tourist arrivals rebounded rapidly. Therefore, in this study, the daily increase in the number of COVID-19 confirmed cases were also considered in the tourism volume forecasting.

The search indexes related to the epidemic were also collected to reflect the people's concerns. The higher the search index value, the higher people's attention and the greater their concerns about travel. These aspects are expected to affect the number of tourists to a certain extent. Thus, in this study, the search engine data related to the epidemic were also analyzed and processed.

(3) Search engine data

Keyword selection from search engines should be broad and reflect the various dimensions of tourism demand, and the selected search keywords should include as much accurate information as possible while eliminating irrelevancies [51]. As Baidu has the largest market share in China, the search engine data were gathered from Baidu. From the keyword selection method mentioned in Sect. 3.1.1, the relevant and frequent keywords are shown in Table 2 and Table 3, and several keywords were finally obtained as shown in Table 4. The Baidu index was collected from its website (https://index.baidu.com/).

In this study, CLSI was used to composite keywords. A synthesized search index not only would contain multidimensional information but could also eliminate the problem of multicollinearity. The tourism-related Baidu index and the epidemic-related Baidu index were synthesized into positive CLSI (Pos-CLSI) and negative CLSI (Neg-CLSI), respectively. Figure 6 shows the sequence diagram of the correlation between tourism volume and the composite search index. The variation trend is roughly the same between tourism volume and Pos-CLSI, whereas the opposite trend can be observed for Neg-CLSI. Regardless of the off-season or peak season, when the people's attention to COVID-19 is high, the amount of tourism has declined significantly. When the people's attention to COVID-19 has declined, the amount of tourism rebounds significantly.

Aiming to reduce the non-stationary characteristics, VMD was conducted to disaggregate the raw CLSI series into several sub-modes. Before VMD was used for the decomposition, the number of sub-modes needed to be determined. On the one hand, if the number of sub-modes is extremely small, then the original sequence may not be fully decomposed, leading to inaccurate predictions. On the other hand, if the signal is over-decomposed, then the difference between each sub-mode will become extremely small, resulting in reduced accuracy and unnecessary computational overhead. Here, the ratio of residual energy r_{res} was used to determine the appropriate number of sub-modes. The equation for calculating r_{res} is shown in Eq. (9). Empirically, when r_{res} is less than 3% and no obvious downward trend is observable, the number of sub-modes can be determined. The r_{res} under the different number of sub-modes is shown in Table 5. The suitable number of sub-modes of the six datasets are 12, 13, 18, 13, 12, and 14, respectively. Take the Pos-CLSI of Huangshan Mountain as an example. Its sub-modes of decomposition results are shown in Fig. 7. The relatively low-frequency sub-modes represent the overall trend of the original CLSI, whereas the higher frequency sub-modes reflect the local fluctuation trend. The extracted sub-sequences are smoother than the raw data, which is conducive to the improvement of tourism volume prediction performance.

After decomposing the CLSI series, the relationship investigation method was conducted to filter out the sub-modes that were conducive to forecasting the tourism volume. Take the tourism volume and tourism-related big data of Huangshan Mountain as an example. The resultant trends can describe the relationship investigation method. The co-integration test and the Granger relationship analysis can only be performed when the time series is stationary. Table 6 shows the results of the stationarity test (i.e., augmented Dickey–Fuller test) and the co-integration tests. Except for S1, the other sub-modes are all stationary with the tourism volume of Huangshan Mountain at the original level. Thereafter, the sub-modes were tested with the tourism volume of Huangshan Mountain for the next step of the co-integration test. Table 6 presents the results for illustrating the co-integration relationships between the tourism volume and sub-modes of Huangshan Mountain other than S2 and S6.

The purpose of adopting Granger causality analysis is to statistically explore whether the sub-modes that pass the co-integration test are beneficial for predicting tourism volume. Table 7 shows that S3, S4, S5, S8, S11, and S16 affect the tourism volume of Huangshan Mountain across one, two, and three orders at the 5% significance level. However, the other sub-modes do not manifest a Granger causality of the

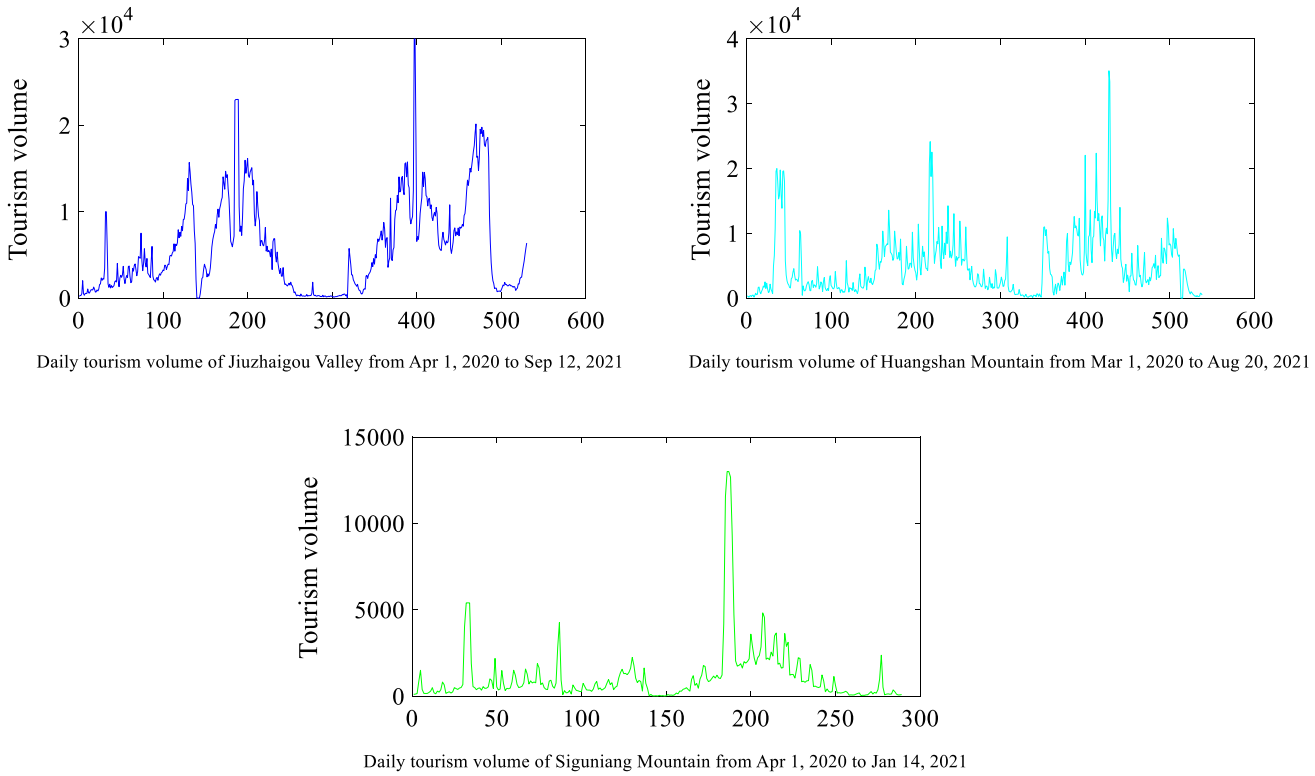

Fig. 4 Daily tourism volume of the three tourist attractions

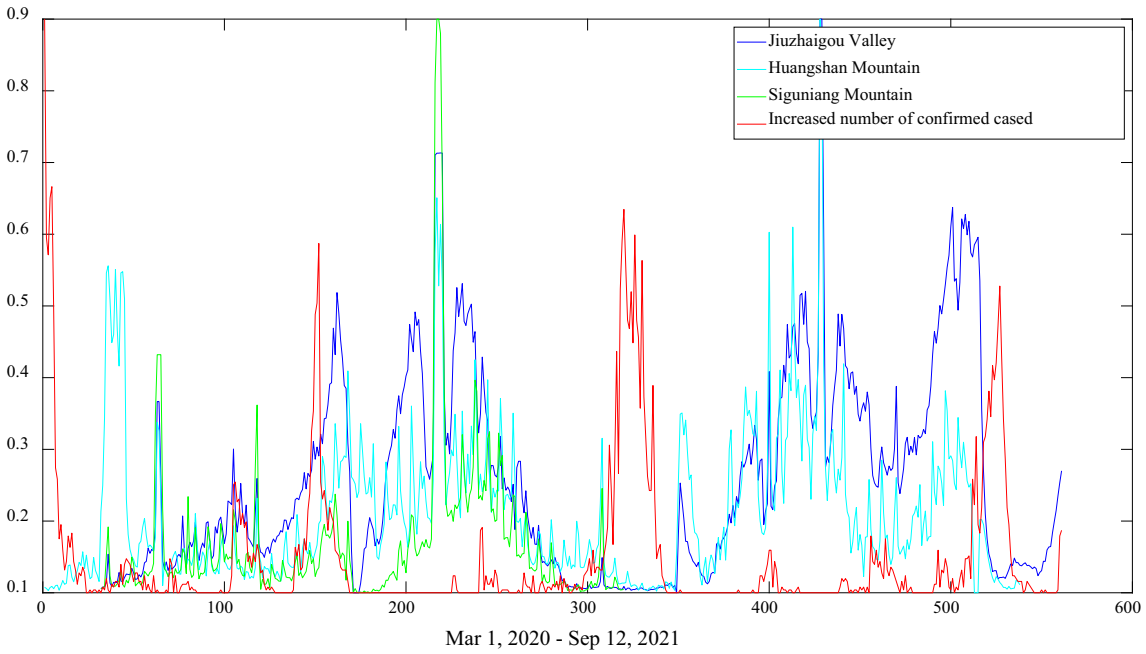

Fig. 5 Time series of increase in confirmed cases and tourism volume of the three tourist attractions

tourism volume. Thus, S3, S4, S5, S8, S11, and S16 were considered for the forecasting of Huangshan Mountain.

Table 8 shows the sub-modes determined by the relationship investigation in each case. Figure 8 illustrates the time series of these selected sub-modes and tourism volume. For the tourism-related sub-modes, the low-frequency sub-modes have a general trend similar to that of tourism volume, whether with a slight lag or contemporarily, and the

Table 2 The relevant and frequent tourism-related keywords in each case

Jiuzhaigou Valley	Huangshan Mountain	Siguniang Mountain
Jiuzhaigou (“九寨沟”)	Huangshan (“黄山”)	Siguniang Mountain (“四姑娘山”)
Weather (“九寨沟天气”)	Weather (“黄山天气”)	Weather (“四姑娘山天气”)
Jiuzhaigou County (“九寨沟县”)	Tourism (“黄山旅游”)	Altitude (“四姑娘山海拔”)
Nuorilang Falls (“诺日朗瀑布”)	Travel guide (“旅游攻略”)	Where is Siguniang Mountain (“四姑娘山在哪里”)
Tourism (“九寨沟旅游”)	Map (“黄山地图”)	Bipengou valley (“毕棚沟”)
Ticket (“九寨沟门票”)	Tourist attractions (“黄山景点”)	Hailuo valley (“海螺沟”)
Travel strategy (“九寨沟旅游攻略”)	Tickets (“黄山门票”)	Gongga Snow Mountain (“贡嘎雪山”)
Five-color lake (“五彩池”)	Scenic area (“黄山风景区”)	Twin bridge trench (“双桥沟”)
Huanglong (“黄龙”)	Travel notes (“黄山游记”)	Dagu Glacier (“达古冰川”)
Where is Jiuzhaigou (“九寨沟在哪”)	Jiuhua Mountain (“九华山”)	Xiling Snow Mountain (“西岭雪山”)
Jiuzhai Huanglong Airport (“九黄机场”)	Huangshan smoke (“黄山烟”)	Daocheng Yading (“稻城亚丁”)
Huanglong tourism (“黄龙旅游”)	Huangshan sea of clouds (“黄山云海”)	Meili Snow Mountain (“梅里雪山”)
Huanglong airport (“黄龙机场”)	Huangshan four unique (“黄山四绝”)	Chengdu to Siguniang Mountain (“成都到四姑娘山”)
Elevation of Jiuzhaigou (“九寨沟海拔”)	Huangshan stone (“黄山奇石”)	Siguniang Mountain Self-driving Tour (“四姑娘山自驾游”)
Huanglong scenic spot (“黄龙风景区”)	Hefei to Huangshan (“合肥到黄山”)	Siguniang Mountain weather forecast (“四姑娘山天气预报”)
Jiuzhaigou Waterfall (“九寨沟瀑布”)	Flying stone (“飞来石”)	Ganzi Prefecture tourism (“甘孜州旅游”)
From Chengdu to Jiuzhaigou Valley (“成都到九寨沟”)	Tour group (“黄山旅游团”)	Moishi Park (“墨石公园”)
Scenery of Jiuzhaigou (“九寨沟风光”)	Hotel (“黄山酒店”)	Qinling Ao Tai (“秦岭鳌太”)
Self-help tour to Jiuzhaigou (“九寨沟自助游”)	Accommodation (“黄山住宿”)	Three peaks of Siguniang Mountain (“四姑娘山三峰”)
The fairy pool (“神仙池”)	Taishan Mountain (“泰山”)	Xiling Snow Mountain tour guide (“西岭雪山导游词”)
Jiuzhaigou Mirror Sea (“九寨沟镜海”)	Which province is Huangshan in (“黄山在哪个省”)	Siguniang Mountain, Sichuan (“四川四姑娘山”)
Is Jiuzhaigou open yet (“九寨沟开放了吗”)	Which city is Huangshan in (“黄山在哪个城市”)	Travel guide (“四姑娘山攻略”)
Jiuzhaigou tourist route (“九寨沟旅游路线”)	Introduction (“黄山简介”)	Tourist attractions in Siguniang Mountain (“四姑娘山景区”)
Pearl Shoal Waterfall (“珍珠滩瀑布”)	Huangshan city (“黄山市”)	Tickets (“四姑娘山门票”)
Sparkling Lake (“火花海”)	Huashan Mountain (“华山”)	Travel (“四姑娘山旅游”)
Jiuzhaigou address (“九寨沟地址”)	The Five Mountains (“五岳”)	Hotel (“四姑娘山住宿”)
Traffic (“九寨沟交通”)	Lu Mountain (“庐山”)	–
Hotel (“九寨沟酒店”)	Huangshan hot spring (“黄山温泉”)	–
Which city is Jiuzhaigou in (“九寨沟在哪个城市”)	Huangshan verse (“黄山诗句”)	–
Weather forecast (“九寨沟天气预报”)	Tiandu Peak (“天都峰”)	–
Map (“九寨沟地图”)	The Pine Greeting Guests (“迎客松”)	–
Jiuzhaigou Introduction (“九寨沟简介”)	Tianzhu Mountain (“天柱山”)	–
Scenic spot (“九寨沟景点”)	Huangshan data (“黄山资料”)	–
Lodging (“九寨沟住宿”)	Huangshan pines (“黄山奇松”)	–
–	Hong village (“宏村”)	–

high-frequency sub-modes produce large fluctuations when the tourist volume fluctuates sharply or when an inflection point occurs. For the epidemic-related sub-modes, the low-frequency sub-modes have a general trend opposite to that

Table 3 The relevant and frequent epidemic-related keywords in each case

Jiuzhaigou Valley	Huangshan Mountain	Siguniang Mountain
Epidemic situation (“疫情”)	Epidemic situation (“疫情”)	Epidemic situation (“疫情”)
Epidemic map (“疫情地图”)	Epidemic map (“疫情地图”)	Epidemic map (“疫情地图”)
Epidemic data (“疫情数据”)	Epidemic data (“疫情数据”)	Epidemic data (“疫情数据”)
Novel coronavirus (“新冠病毒”)	Novel coronavirus (“新冠病毒”)	Novel coronavirus (“新冠病毒”)
COVID-19 vaccine (“新冠疫苗”)	COVID-19 vaccine (“新冠疫苗”)	COVID-19 vaccine (“新冠疫苗”)
Vaccine (“疫苗”)	Vaccine (“疫苗”)	Vaccine (“疫苗”)
Epidemic prevention and control (“疫情防控”)	Epidemic prevention and control (“疫情防控”)	Epidemic prevention and control (“疫情防控”)
Epidemic in Sichuan province (“四川疫情”)	Epidemic in Anhui Province (“安徽疫情”)	Epidemic in Sichuan Province (“四川疫情”)
Epidemic in Guangdong province (“广东疫情”)	Epidemic in Jiangsu Province (“江苏疫情”)	Epidemic in Guangdong Province (“广东疫情”)
Epidemic in Jiangsu Province (“江苏疫情”)	Epidemic in Zhejiang Province (“浙江疫情”)	Epidemic in Chongqing Province (“重庆疫情”)
Epidemic in Shandong Province (“山东疫情”)	Epidemic in Guangdong Province (“广东疫情”)	Updated list of mid- and high-risk areas (“疫情中高风险地区最新名单”)
Epidemic in Shanghai Province (“上海疫情”)	Epidemic in Shandong Province (“山东疫情”)	Epidemic risk areas (“疫情风险地区”)
Epidemic in Beijing Province (“北京疫情”)	Epidemic in Shanghai Province (“上海疫情”)	Medium and high risk areas (“中高风险地区”)
Epidemic in Henan Province (“河南疫情”)	Epidemic in Beijing Province (“北京疫情”)	Epidemic risk level query (“疫情风险等级查询”)
Epidemic in Hebei Province (“河北疫情”)	Epidemic in Henan Province (“河南疫情”)	Risk area (“风险地区”)
Updated list of mid- and high-risk areas (“疫情中高风险地区最新名单”)	Epidemic in Hebei Province (“河北疫情”)	Novel coronavirus mutations (“新冠病毒变异”)
Epidemic risk areas (“疫情风险地区”)	Epidemic in Sichuan Province (“四川疫情”)	Domestic epidemic (“国内疫情”)
Medium and high risk areas (“中高风险地区”)	Updated list of mid- and high-risk areas (“疫情中高风险地区最新名单”)	The latest data news of the epidemic (“疫情最新数据消息”)
Epidemic risk level query (“疫情风险等级查询”)	Epidemic risk areas (“疫情风险地区”)	–
Risk area (“风险地区”)	Medium and high risk areas (“中高风险地区”)	–
Novel coronavirus mutations (“新冠病毒变异”)	Epidemic risk level query (“疫情风险等级查询”)	–
Domestic epidemic (“国内疫情”)	Risk area (“风险地区”)	–
The latest data news of the epidemic (“疫情最新数据消息”)	Novel coronavirus mutations (“新冠病毒变异”)	–
–	Domestic epidemic (“国内疫情”)	–
–	The latest data news of the epidemic (“疫情最新数据消息”)	–

of tourism volume. Its high-frequency sub-modes fluctuate sharply when the attention of the epidemic changes drastically.

(4) Weather data

The weather data of the three tourist attractions, which were collected from the Tianqi website, include weather condition data and temperature data, as shown in Fig. 9. According to their impact on travel, the weather conditions were transformed into dummy variables, i.e., a degree of impact from one to six levels.

4.2 Tourism volume forecasting

(a) Forecasting procedure

The three datasets were partitioned into three sets, namely the training, validation, and test sets (Table 9). The training set, validation set, and test set accounted for approximately

Table 4 Keywords identified and their maximum TDC ($1 \leq l \leq 3$) in each case

	Jiuzhaigou Valley		Huangshan Mountain		Siguniang Mountain	
	Keywords	TDC	Keywords	TDC	Keywords	TDC
Tourism-related keywords	Weather (“九寨沟天气”)	$0.858^{**}, l = 2$	Travel guide (“黄山旅游攻略”)	$0.712^{**}, l = 2$	Twin bridge trench (“双桥沟”)	$0.799^{**}, l = 1$
	Jiuzhaigou (“九寨沟”)	$0.808^{**}, l = 1$	Map (“黄山地图”)	$0.707^{**}, l = 1$	Weather (“四姑娘山天气”)	$0.782^{**}, l = 2$
	Nuorilang Falls (“诺日朗瀑布”)	$0.744^{**}, l = 1$	Huangshan (“黄山”)	$0.704^{**}, l = 1$	Bipengou valley (“毕鹏沟”)	$0.764^{**}, l = 2$
	Tourism (“九寨沟旅游”)	$0.741^{**}, l = 3$	Tickets (“黄山门票”)	$0.679^{**}, l = 3$	Siguniang Mountain (“四姑娘山”)	$0.707^{**}, l = 2$
	Five-color lake (“五彩池”)	$0.737^{**}, l = 1$	Tourist attractions (“黄山景点”)	$0.671^{**}, l = 1$	Altitude (“四姑娘山海拔”)	$0.668^{**}, l = 2$
	Where is Jiuzhaigou (“九寨沟在哪”)	$0.673^{**}, l = 1$	Tourism (“黄山旅游”)	$0.645^{**}, l = 3$	–	–
	Huanglong (“黄龙”)	$0.657^{**}, l = 1$	From Hefei to Huangshan (“合肥到黄山”)	$0.639^{**}, l = 3$	–	–
	Travel strategy (“九寨沟旅游攻略”)	$0.617^{**}, l = 3$	Jiuhua Mountain (“九华山”)	$0.638^{**}, l = 1$	–	–
Epidemic-related keywords	Epidemic prevention and control (“疫情防控”)	$-0.471^{**}, l = 1$	Epidemic prevention and control (“疫情防控”)	$-0.340^{**}, l = 1$	Epidemic prevention and control (“疫情防控”)	$-0.320^{**}, l = 1$
	Epidemic map (“疫情地图”)	$-0.461^{**}, l = 3$	COVID-19 (“新冠病毒”)	$-0.313^{**}, l = 2$	Epidemic situation (“疫情”)	$-0.259^{**}, l = 1$
	Epidemic situation (“疫情”)	$-0.459^{**}, l = 3$	Epidemic situation (“疫情”)	$-0.309^{**}, l = 1$	Vaccine (“疫苗”)	$-0.255^{**}, l = 1$
	Epidemic data (“疫情数据”)	$-0.367^{**}, l = 1$	Epidemic map (“疫情地图”)	$-0.238^{**}, l = 1$	COVID-19 (“新冠病毒”)	$-0.250^{**}, l = 1$
	Novel coronavirus (“新冠病毒”)	$-0.299^{**}, l = 3$	Epidemic data (“疫情数据”)	$-0.221^{**}, l = 1$	Epidemic map (“疫情地图”)	$-0.236^{**}, l = 1$
	–	–	Epidemic in Jiangsu Province (“江苏疫情”)	$-0.212^{**}, l = 3$	Epidemic data (“疫情数据”)	$-0.229^{**}, l = 1$

**Tourism volume and keywords have a significant correlation at the 1% level (two-tailed)

70%, 10%, and 20% of the total datasets, respectively. The training and validation sets were used to adjust the parameters of the forecasting models. Thereafter, the training and validation sets were combined to train the forecasting model, whereas the test set was used to test the forecasting performance. The tourism volume forecasting models all implemented the rolling window method.

(b) Parameter set

For a fair comparison, the DE algorithm was used to determine the optimal parameters of BPNN, SVM, RNN, GRU, and LSTM. The grid search method was used to optimize the parameters of DE. The parameters of the different comparable models are listed in Table 10.

The search range of TFT parameters is as follows: the range of time step is [2, 12], the range of batch size is [12, 48], and the range of learning rate is [0.001, 0.1], the range of the number of hidden layers is [2, 16], the range of the number of attention heads is [1, 4], the range of the number of consecutive hidden layers is [2, 8]. The determined parameters of DE-TFT are shown in Table 11. To show the types of input data of the TFT model more clearly, taking Jiuzhaigou Valley as an example, Table 12 shows the input variables contained in different input types. Because the historical data of known future variables are also known, the known future variables are also input into the TFT model as past variables. To eliminate the effect of 0 values on the calculation, all input variables and tourism volume data were scaled between 0.1 and 0.9.

The program running speed of TFT is about 35 s every time. The running speed of DE-TFT is mainly determined by the iteration number and population size of the DE algorithm. In this study, the running times of the Jiuzhaigou

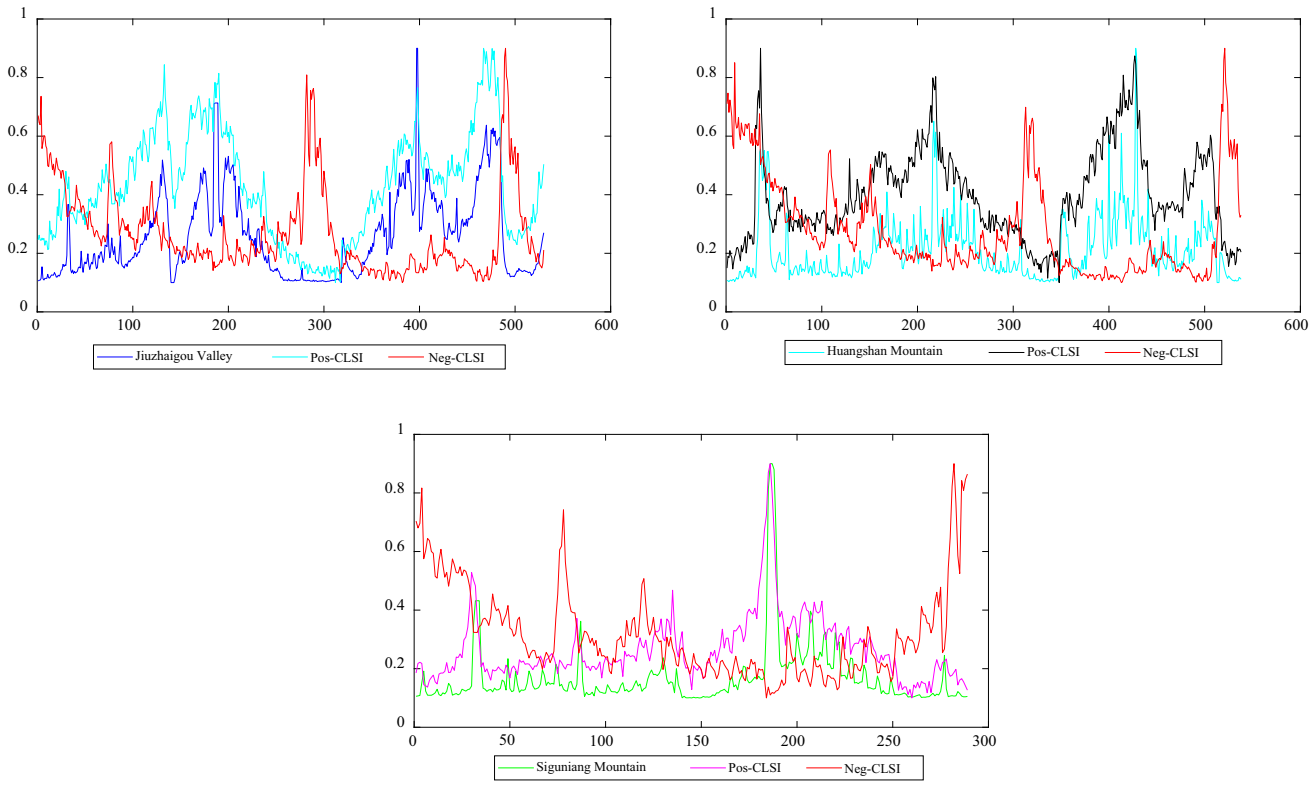

Fig. 6 Time series of CLSI and tourism volume of the three tourist attractions

Table 5 r_{res} corresponding to the different number of sub-modes

K	Jiuzhaigou (r_{res}, %)		Huangshan Mountain (r_{res}, %)		Siguniang Mountain (r_{res}, %)	
	Pos-CLSI	Neg-CLSI	Pos-CLSI	Neg-CLSI	Pos-CLSI	Neg-CLSI
2	7.53	12.24	14.47	11.05	11.92	12.23
3	7.14	10.60	10.70	7.71	8.52	11.44
4	4.76	10.47	10.21	7.48	8.26	11.26
5	4.49	6.59	7.85	6.19	7.02	7.81
6	4.13	4.92	6.18	5.89	6.69	7.34
7	3.93	4.80	5.97	5.75	5.53	7.24
8	3.02	4.52	4.72	4.74	4.06	4.83
9	2.91	4.43	4.48	4.67	3.89	4.66
10	2.69	3.20	3.94	3.13	3.21	4.40
11	2.59	3.08	3.80	3.05	3.01	4.30
12	**1.97**	2.52	3.44	3.00	**2.73**	3.27
13	1.93	**2.05**	3.30	**2.33**	2.69	3.17
14	1.82	1.95	3.11	2.27	2.08	**2.28**
15	1.80	1.90	3.07	1.94	2.04	2.25
16	1.76	1.73	2.54	1.87	1.69	2.12
17	1.30	1.65	2.52	1.59	1.53	2.12
18	1.26	1.63	**2.08**	1.56	1.49	2.05
19	1.25	1.40	2.04	1.43	1.44	2.02
20	1.23	1.38	2.03	1.42	1.44	1.95

Bold values indicate r_{res} corresponding to the optimal number of submodes

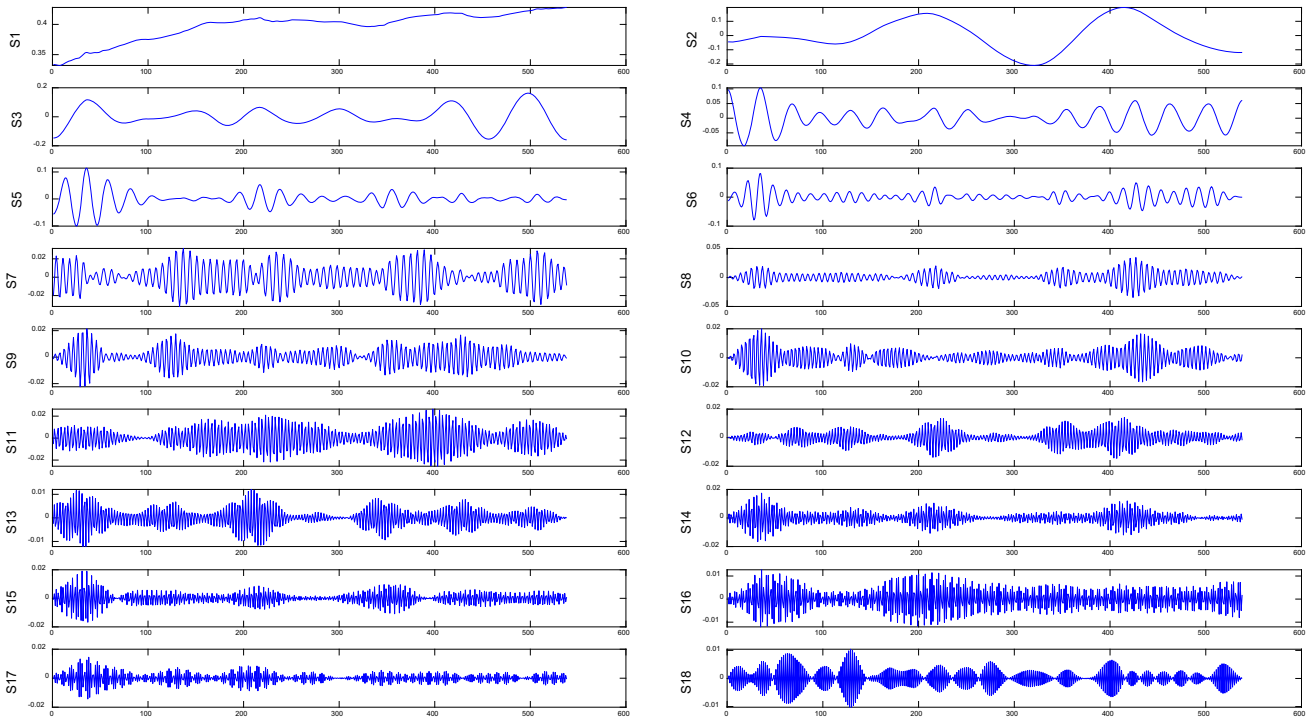

Fig. 7 Decomposition results by VMD for Pos-CLSI of Huangshan Mountain

Table 6 Test results of the stationarity test and the co-integration tests at a 5% level

Time series (at the original level)	The stationarity test	The cointegration tests
Huangshan Mountain tourism volume	− 3.9831 (**0.015**)	–
S1	− 2.4202 (0.1361)	–
S2	− 4.2879 (**0.0005**)	− 2.155 (0.4474)
S3	− 8.3233 (**0.0000**)	− 5.6615 (**0.0000**)
S4	− 8.7390 (**0.0000**)	− 13.3305 (**0.0000**)
S5	− 10.2239 (**0.0000**)	− 8.1316 (**0.0000**)
S6	− 10.1061 (**0.0000**)	− 3.3338 (0.0503)
S7	− 11.3783 (**0.0000**)	− 4.5010 (**0.0012**)
S8	− 9.9999 (**0.0000**)	− 3.9973 (**0.0072**)
S9	− 8.5458 (**0.0000**)	− 3.9632 (**0.0080**)
S10	− 10.0238 (**0.0000**)	− 3.6417 (**0.0217**)
S11	− 8.8418 (**0.0000**)	− 3.5702 (**0.0266**)
S12	− 10.1864 (**0.0000**)	− 3.6532 (**0.0210**)
S13	− 8.8741 (**0.0000**)	− 3.7654 (**0.0150**)
S14	− 8.5955 (**0.0000**)	− 3.7944 (**0.0137**)
S15	− 8.3070 (**0.0000**)	− 3.8859 (**0.0103**)
S16	− 8.0741 (**0.0000**)	− 4.3564 (**0.0020**)
S17	− 10.2667 (**0.0000**)	− 5.7541 (**0.0000**)
S18	− 10.6150 (**0.0000**)	− 3.5857 (**0.0255**)

Bold value indicate that the result is significant at a 5% level

dataset, Huangshan dataset, and Siguniangshan dataset are about 230 min, 350 min, and 300 min, respectively.

(iii) Results and discussion

The comparison of the forecasting models depicting the forecasting accuracies of the three tourist attractions using all input data is shown in Table 13 and Fig. 10. The results indicate that the DE-TFT model has the best forecasting

Table 7 Test results of the Granger causality analysis at 5% level

Lags	1	2	3
Panel A	H0: S3 does not Granger cause Huangshan Mountain tourism volume		
F-stat (*p* value)	14.0818 (**0.0002**)	7.1235 (**0.0008**)	5.1623 (**0.0016**)
Panel B	H0: S4 does not Granger cause Huangshan Mountain tourism volume		
F-stat (*p* value)	9.4198 (**0.0023**)	5.7909 (**0.0033**)	3.9786 (**0.0080**)
Panel C	H0: S5 does not Granger cause Huangshan Mountain tourism volume		
F-stat (*p* value)	10.8125 (**0.0011**)	6.2854 (**0.0020**)	4.3419 (**0.0049**)
Panel D	H0: S7 does not Granger cause Huangshan Mountain tourism volume		
F-stat (*p* value)	2.6024 (0.1073)	–	–
Panel E	H0: S8 does not Granger cause Huangshan Mountain tourism volume		
F-stat (*p* value)	15.2964 (**0.0001**)	7.7163 (**0.0004**)	5.1636 (**0.0016**)
Panel *F*	H0: S9 does not Granger cause Huangshan Mountain tourism volume		
F-stat (*p* value)	1.7755 (0.1833)	–	–
Panel G	H0: S10 does not Granger cause Huangshan Mountain tourism volume		
F-stat (*p* value)	1.2189 (0.2701)	–	–
Panel H	H0: S11 does not Granger cause Huangshan Mountain tourism volume		
F-stat (*p* value)	28.5279 (**1.3681e-07**)	16.2620 (**1.3939e-07**)	10.9049 (**5.8238e-07**)
Panel I	H0: S12 does not Granger cause Huangshan Mountain tourism volume		
F-stat (*p* value)	1.2632 (0.2616)	–	–
Panel J	H0: S13 does not Granger cause Huangshan Mountain tourism volume		
F-stat (*p* value)	0.8664 (0.3524)	–	–
Panel K	H0: S14 does not Granger cause Huangshan Mountain tourism volume		
F-stat (*p* value)	1.3925 (0.2385)	–	–
Panel L	H0: S15 does not Granger cause Huangshan Mountain tourism volume		
F-stat (*p* value)	0.2343 (0.6285)	–	–
Panel M	H0: S16 does not Granger cause Huangshan Mountain tourism volume		
F-stat (*p* value)	8.2800 (**0.0042**)	6.5877 (**0.0015**)	4.8314 (**0.0025**)
Panel N	H0: S17 does not Granger cause Huangshan Mountain tourism volume		
F-stat (*p* value)	0.1501 (0.6985)	–	–
Panel O	H0: S18 does not Granger cause Huangshan Mountain tourism volume		
F-stat (*p* value)	0.3159 (0.5743)	–	–

Bold value indicate that the result is significant at a 5% level

Table 8 Sub-modes were identified in each case

	Jiuzhaigou (r_{res}, %)		Huangshan Mountain (r_{res}, %)		Siguniang Mountain (r_{res}, %)	
	Pos-CLSI	Neg-CLSI	Pos-CLSI	Neg-CLSI	Pos-CLSI	Neg-CLSI
Sub-modes identified	S2, S9	S2	S3, S4, S5, S8, S11, S16	S8	S2, S3, S4, S6	S9

accuracy for Jiuzhaigou Valley in contrast to DE-BPNN, DE-SVM, DE-LSTM, DE-GRU, and DE-RNN. In terms of MAPE, the results of DE-TFT are improved by 56.14%, 77.82%, 50.78%, 59.71%, and 44.12% over DE-BPNN, DE-SVM, DE-LSTM, DE-RNN, DE-GRU, respectively. In particular, the forecasting results of DE-TFT are closer to the actual tourism volume, especially when the tourism volume fluctuates greatly.

As a means of verifying whether the historical tourism volume data, increase in confirmed cases, weather data, tourism-related search engine data, and epidemic-related search engine data can enhance the forecasting accuracy of tourism volume, we further use "historical tourism volume data," "historical tourism volume data + increase in confirmed cases, "historical tourism volume data + increase in confirmed cases + weather data," "historical tourism volume

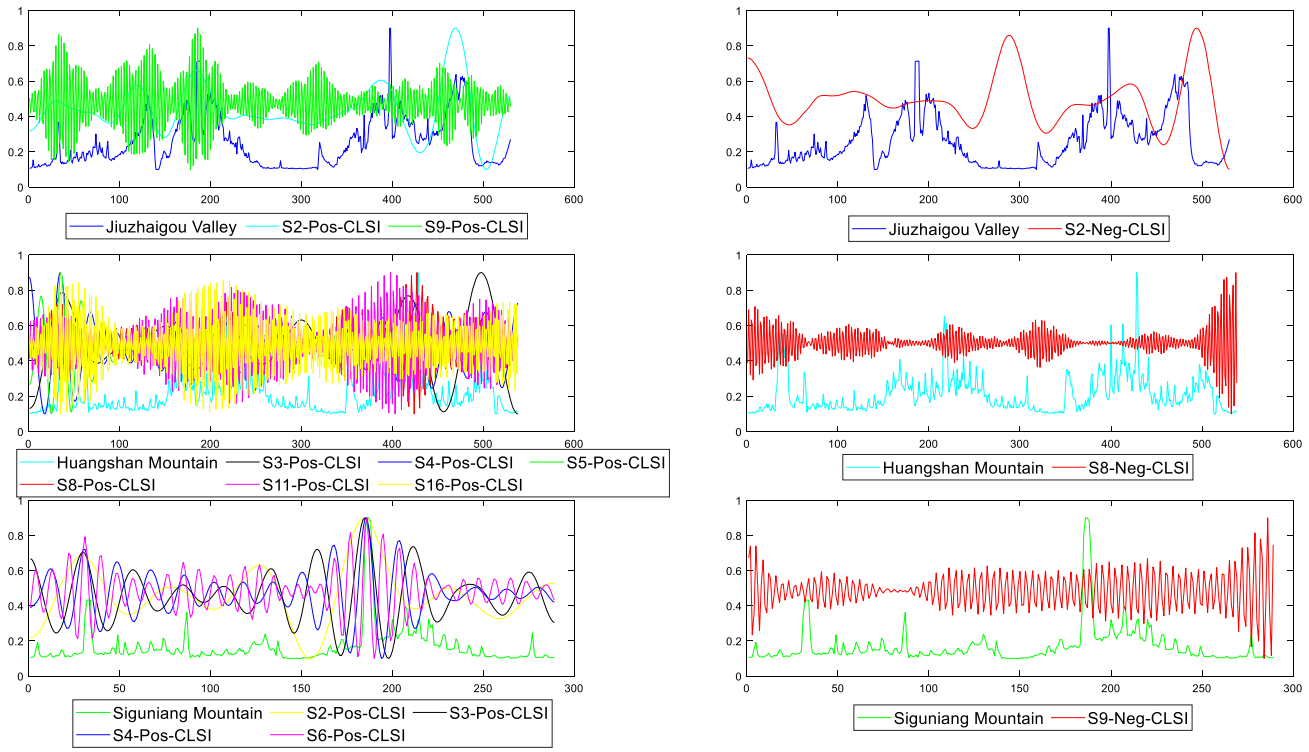

Fig. 8 Time series of determined sub-modes and tourism volume of the three tourist attractions

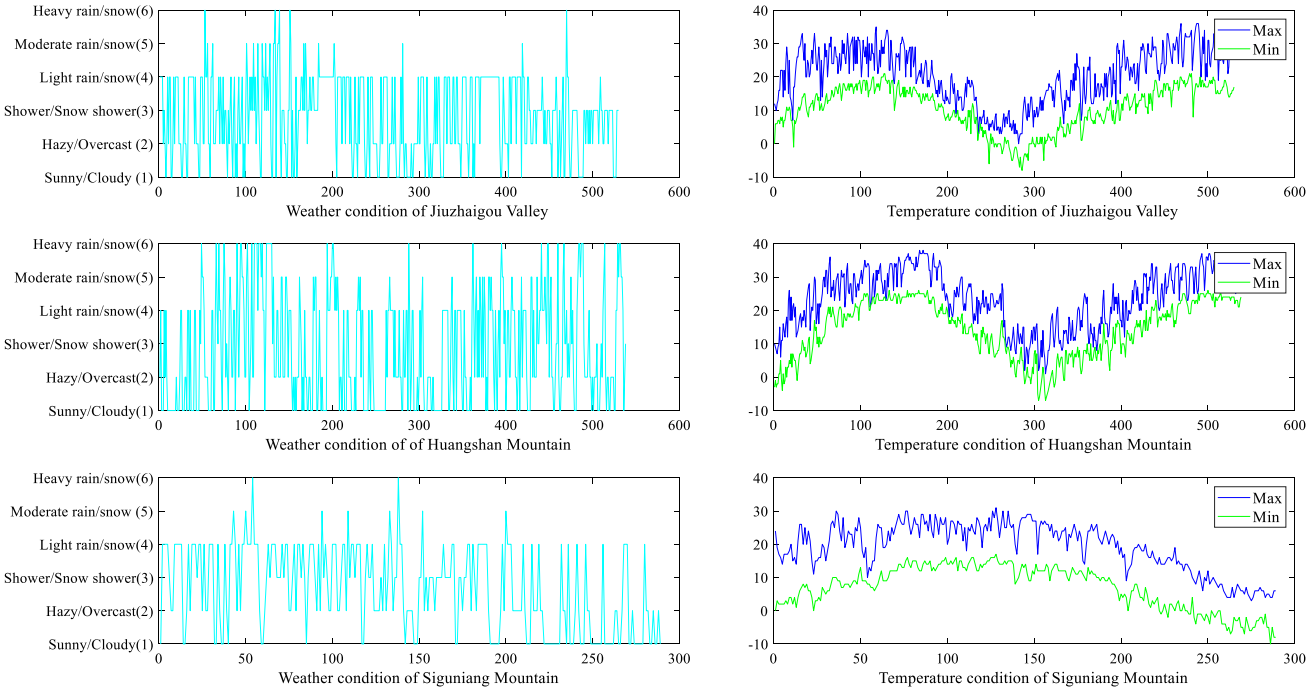

Fig. 9 Daily weather and temperature conditions of the three tourist attractions

data + increase in confirmed cases + weather data + tourism-related search engine data" and "historical tourism volume data + increase in confirmed cases + weather data + tourism-related search engine data + epidemic-related search engine data," respectively, as the independent variables of the three cases. The performance of different variable combinations is shown in Table 14.

Table 9 Training, validation, and test sets of the three cases

	Training set	Validation set	Test set
Jiuzhaigou Valley	Apr 1, 2020-Mar 31, 2021 (A total of 365 days)	Apr 1, 2021- May 31, 2021 (A total of 61 days)	Jun 1, 2021- Sep 12, 2021 (A total of 104 days)
Huangshan Mountain	Mar 1, 2020-Mar 11, 2021 (A total of 376 days)	Mar 12, 2021-Apr 30, 2021 (A total of 50 days)	May 1, 2021- Aug 20, 2021 (A total of 112 days)
Siguniang Mountain	Apr 1, 2020-Oct 20, 2020 (A total of 203 days)	Oct 21, 2020-Nov 20, 2020 (A total of 31 days)	Nov 21, 2020-Jan 14, 2021 (A total of 55 days)

Table 10 Parameters of the different models

Model and variable	Adopted parameters		
	Jiuzhaigou Valley	Huangshan Mountain	Siguniang Mountain
DE-BPNN	Hidden neurons=6; Learning rate=0.005; Epochs=201	Hidden neurons=8; Learning rate=0.051; Epochs=249	Hidden neurons=6; Learning rate=0.008; Epochs=168
DE-SVM	Kernel="rbf"; Gamma=0.11; C=3.01	Kernel="rbf"; Gamma=0.20; C=2.59	Kernel="rbf"; Gamma=0.12; C=1.51
DE-LSTM	batch size=32; hidden Neurons=26; epochs=241; time step=9	Batch size=33; hidden Neurons=30; epochs=245; time step=7	Batch size=15; hidden Neurons=26; epochs=302; time step=8
DE-GRU	Batch size=31; hidden Neurons=25; epochs=233; time step=9	Batch size=30; hidden Neurons=28; epochs=241; time step=7	Batch size=14; hidden Neurons=21; epochs=301; time step=8
DE-RNN	Batch size=38; hidden Neurons=21; epochs=245; time step=9	Batch size=35; hidden Neurons=32; epochs=245; time step=7	Batch size=14; hidden Neurons=21; epochs=235; time step=8

Table 11 Parameters of the DE-TFT in the three data sets

	Parameter	Jiuzhaigou Valley	Huangshan Mountain	Siguniang Mountain
DE	Population size (M)	15	15	20
	Maximum number of iterations (T)	20	30	25
	Crossover probability (CR)	0.2	0.4	0.6
	Mutation operator (F)	0.3	0.2	0.3
TFT	Number of time steps	9	7	8
	Number of batch sizes	31	30	28
	Learning rates	0.098	0.092	0.051
	Number of hidden layers	16	13	8
	Number of attention heads	1	1	1
	Number of consecutive hidden layers	8	7	4
	Dropout rate	0.1	0.1	0.1
	Max gradient norm	0.1	0.1	0.1

The forecasting performance of "historical tourism volume data + increase in confirmed cases + weather data + tourism-related search engine data + epidemic-related search engine data" is better than those of the other variable combinations for the three tourist attractions. The results demonstrate the validity and superiority of using multisource big data in improving the performance of tourism demand forecasting under the impact of COVID-19.

Further aiming to verify the role of the composite and decomposition indexes in tourism volume forecasting, this study compared the various forecasting situations that do not deal with the search index. CLSI was used for the

Table 12 Inputs of the DE-TFT in the Jiuzhaigou Valley

Static covariates	Past inputs	Known future inputs
ID (name of tourism volume series)	Weather condition data	Weather condition data
–	Max temperature data	Max temperature data
–	Min temperature data	Min temperature data
–	Day	Day
–	Month	Month
–	Increased confirmed cases	Time index
–	Historical tourism volume data	Relative time index
–	Pos-CLSI-S2	–
–	Pos-CLSI-S9	–
–	Neg-CLSI-S2	–
–	Time index	–
–	Relative time index	–

Table 13 Forecasting accuracy of each model

Model	Jiuzhaigou Valley			Huangshan Mountain			Siguniang Mountain		
	MAPE (%)	MAE	RMSE	MAPE (%)	MAE	RMSE	MAPE (%)	MAE	RMSE
DE-BPNN	11.49	0.0317	0.0434	13.24	0.0319	0.0547	9.62	0.0137	0.0241
DE-SVM	22.72	0.0618	0.0832	27.72	0.0627	0.0998	13.41	0.0167	0.0211
DE-LSTM	10.24	0.0275	0.0409	12.92	0.0332	0.0611	11.16	0.0150	0.0229
DE-RNN	12.51	0.0384	0.0542	12.34	0.0319	0.0610	9.42	0.0142	0.0270
DE-GRU	9.02	0.0232	0.0338	13.64	0.0346	0.0624	12.82	0.0172	0.0254
DE-TFT	**5.04**	**0.0136**	**0.0179**	**8.59**	**0.0190**	**0.0263**	**5.89**	**0.0081**	**0.0120**

Bold values indicate best forecasting performance

aggregate search index, and then VMD, EMD, and EEMD were utilized for further decomposition. As shown in Table 15, on the one hand, using the CLSI method can obtain better forecasting performance than the use of raw search engine data concerning the three tourist attractions. On the other hand, VMD can obtain a better decomposition effect than EMD and EEMD.

(iv) Interpretable results

Figure 11 shows the interpretable results of the DE-TFT model, which are primarily categorized into three parts: the importance ranking of past inputs, the importance ranking of future variables, and the attention of different lag orders. The specific analysis is as follows:

- The analysis of the importance of past inputs suggests that historical tourism volume data and tourism-related search indexes are most helpful to tourism forecasting. On the other hand, it demonstrates that the epidemic-related search index has played a more pivotal role in forecasting than the daily increased confirmed cases. This finding can be attributed to the fact that the epidemic-related search engine data can reflect travelers' concerns more objectively than the daily increased confirmed cases. Besides, concerns about the COVID-19 epidemic at that time affected travelers' travel plans. The locally newly confirmed cases may only reflect the local situation, incapable of fully reflecting the concerns about the epidemic nationwide.
- Regarding the importance of known variables, various weather conditions including both the max and min temperature can be conducive to the forecast of tourism demand, of which the temperature factor accounts for the main contribution, indicating that the tourism season is closely related to the season. Generally speaking, travelers will choose to travel when the temperature is suitable. Based on the data on the number of tourists and weather conditions in these three scenic spots, it can be concluded that bad weather will be followed by a sharp drop in the daily number of tourists in each scenic spot.
- Interpretability results show that the general trend of attentional changes is that the smaller the lag order, the greater the contribution to tourism demand forecasting. However, larger lag sequences are sometimes also

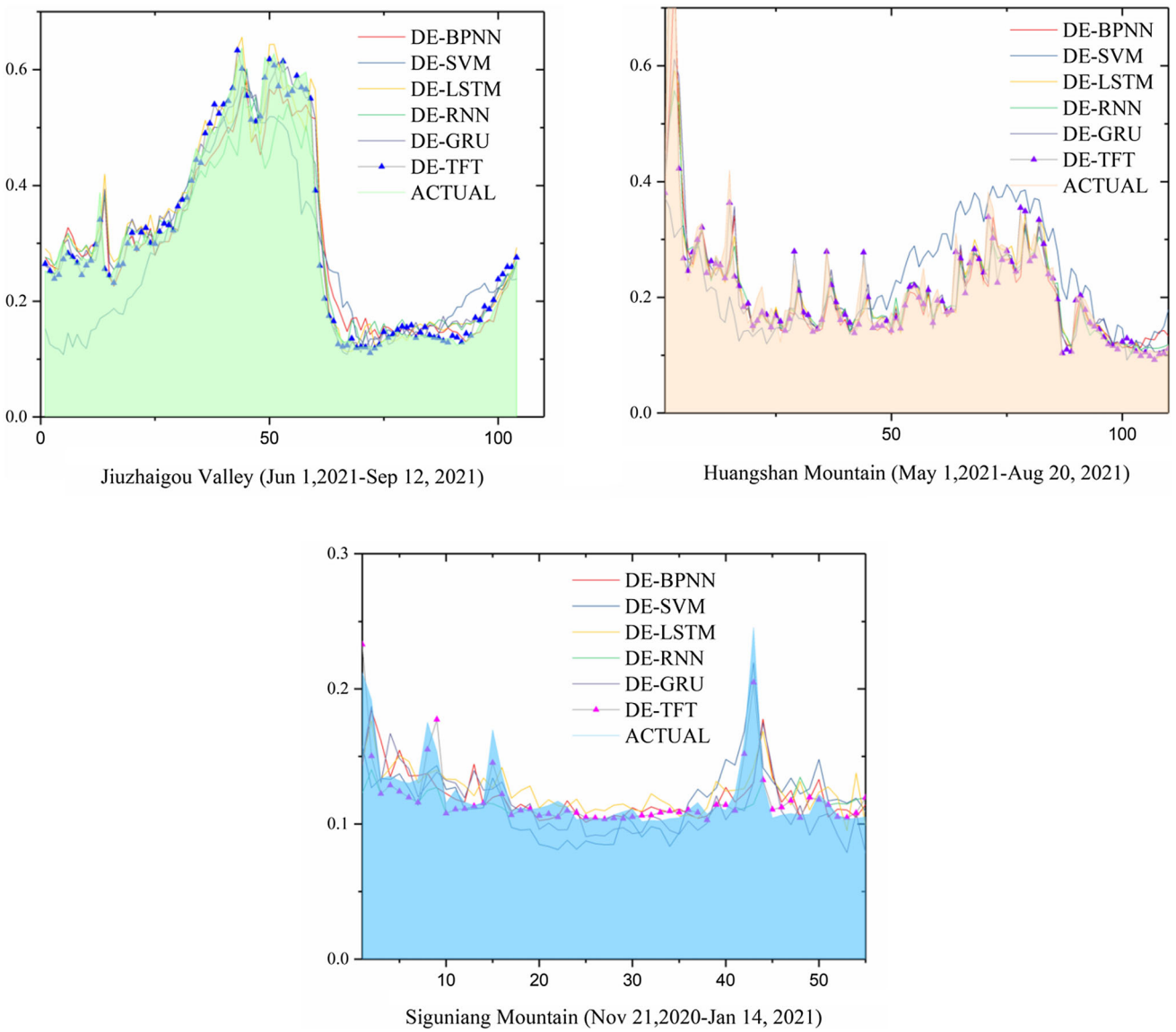

Fig. 10 Forecasting results of the DE-TFT and other comparable models

Table 14 Forecasting accuracy of different kinds of variables

Variable	Jiuzhaigou Valley using DE-TFT			Huangshan Mountain using DE-TFT			Siguniang Mountain using DE-TFT		
	MAPE (%)	MAE	RMSE	MAPE (%)	MAE	RMSE	MAPE (%)	MAE	RMSE
1	9.32	0.0216	0.0421	14.51	0.0361	0.0783	14.07	0.0184	0.0262
1+2	7.67	0.0197	0.0437	14.38	0.0354	0.0663	12.46	0.0153	0.0267
1+2+3	6.89	0.0179	0.0283	13.37	0.0345	0.0643	11.57	0.0140	0.0259
1+2+3+4	6.51	0.0169	0.0229	11.92	0.0295	0.0534	10.70	0.0128	0.0253
1+2+3+4+5	**5.04**	**0.0136**	**0.0179**	**8.59**	**0.0190**	**0.0263**	**5.89**	**0.0081**	**0.0120**

"1" denotes historical tourism volume data. "2" denotes an increase in confirmed cases. "3" denotes weather data. "4" denotes tourism-related search engine data. "5" denotes epidemic-related search engine data. Bold values indicate the best forecasting performance

Table 15 Forecasting accuracy with different ways to handle the search engine data

Variable	Jiuzhaigou Valley using DE-TFT			Huangshan Mountain using DE-TFT			Siguniang Mountain using DE-TFT		
	MAPE (%)	MAE	RMSE	MAPE (%)	MAE	RMSE	MAPE (%)	MAE	RMSE
Without CLSI-VMD	10.78	0.0307	0.0442	14.19	0.0346	0.0659	14.30	0.0188	0.0275
CLSI	10.43	0.0314	0.0448	12.80	0.0331	0.0619	9.20	0.0146	0.0332
CLSI-EMD	11.37	0.0322	0.0511	13.72	0.0346	0.0629	11.66	0.0145	0.0210
CLSI-EEMD	6.55	0.0181	0.0325	12.42	0.0319	0.0612	11.75	0.0142	0.0259
CLSI-VMD	**5.04**	**0.0136**	**0.0179**	**8.59**	**0.0190**	**0.0263**	**5.89**	**0.0081**	**0.0120**

Bold values indicate the best forecasting performance

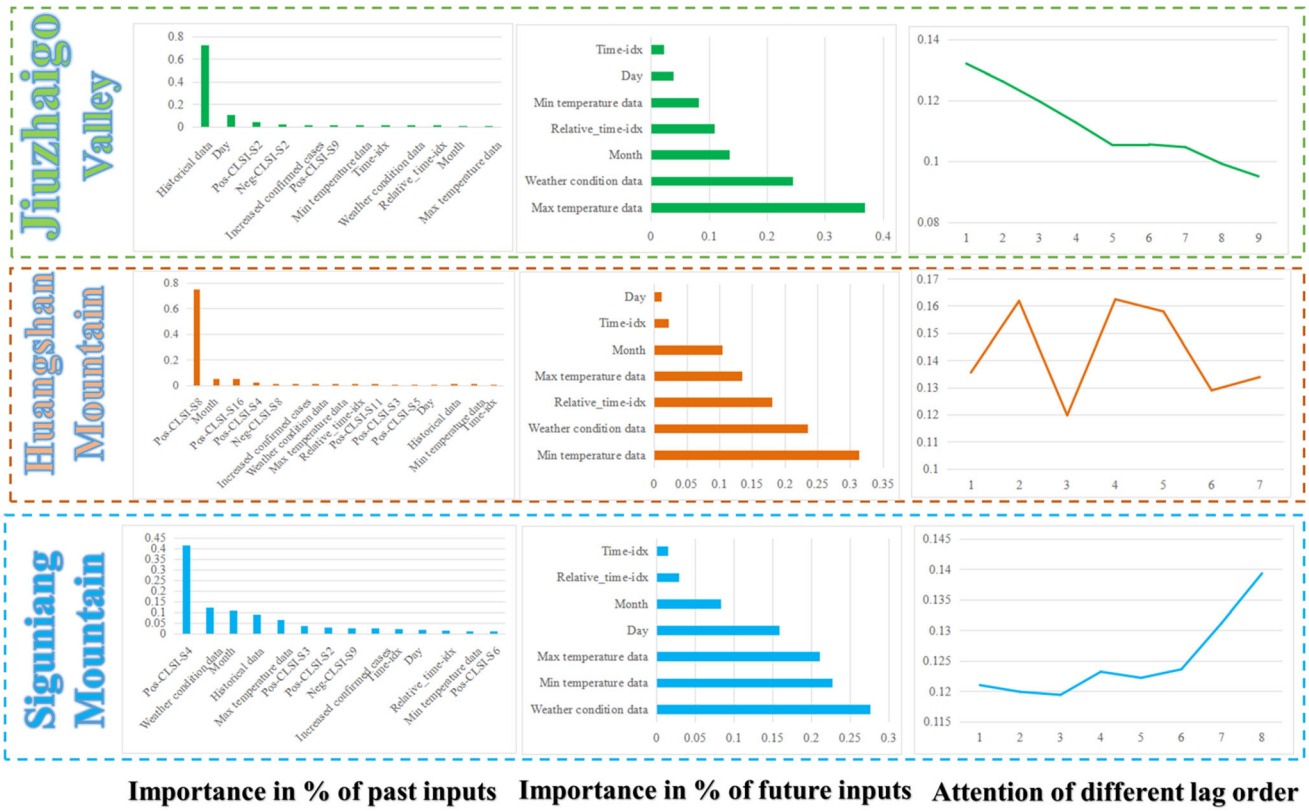

Fig. 11 Interpretable results of the DE-TFT model in three data sets

related to larger attention. For example, in the Siguniang Mountain dataset, the longer the lag order, the higher the attention. Therefore, it requires the prediction model to be equipped with the memory ability to retrieve long-term input, thereby making it particularly important to determine the appropriate lag order, which also proves the necessity of optimizing the TFT parameters proposed in this study via DE.

5 Conclusion and implications

The objective of this study is to construct a comprehensive interpretable forecasting framework to forecast daily tourism demand under the impact of COVID-19. A novel approach that can simultaneously use historical tourism volume data, daily increase in confirmed cases, weather data, tourism-related search engine data, and epidemic-related search engine data was used to forecast the daily tourism volume of Jiuzhaigou Valley, Huangshan Mountain, and Siguniang Mountain—the three famous tourist

attractions in China. Moreover, this study introduced the concept of epidemic-related search indexes, thus offering new insights into tourism forecasting during the COVID-19 pandemic. In particular, a new search engine data processing method called CLSI-VMD was utilized.

The contributions of the study are multifaceted, and the specific contributions are as follows: Firstly, to the best of our knowledge, our research is the first to incorporate tourism attention, epidemic situation, and weather conditions into tourism demand forecasting during the COVID-19 pandemic. Multi-source data can provide a much stronger theory and a more comprehensive overview for tourism volume forecasting. Secondly, a novel interpretable forecasting model, DE-TFT, is proposed, which can better improve the performance of tourism demand forecasting and explain the role of input variables. The DE algorithm is used to optimize the parameter combination of the TFT model, which improves the performance and stability of the model. The interpretability analysis of tourism demand forecasts can also provide more persuasive analysis to tourism-related decision-makers, helping them to make more accurate forecasts and make more reliable plans. Thirdly, this study has introduced a new keyword category —the epidemic-related keywords—to forecast tourism demand under the impact of COVID-19. The experimental results indicate that the epidemic-related search engine data can better improve the forecasting performance compared with the general epidemic data (e.g., daily increase in confirmed cases), further implying that the concerns of tourists about tourism during the COVID-19 epidemic can be better reflected. Fourthly, this study has proposed a new CLSI–VMD method to process the search engine data (e.g., Google Trends and Baidu index) and provided a novel perspective on tourism demand forecasting by exploring decomposition methods in extracting the sub-modes of composite search engine data.

Our work has practical implications for managers of tourism destinations and attractions. Firstly, the recurrence of epidemics has caused large fluctuations in tourism demand, and the effects cannot be judged by solely relying on the traditional off-season and peak seasons, which are the information generally used in the past. Our proposed approach highlights the importance of epidemic-related data, allowing for the improved accuracy of tourism demand forecasting during the COVID-19 epidemic. Thus, tourism authorities can apply tourism demand forecasting to support crowd management and better guard against COVID-19 in the long run. Secondly, tourist site operators can judge the impact of the epidemic based on the number of tourists by using the search index related to the epidemic rather than the number of new epidemics, as the former can better reflect the concerns of tourists. Finally, the high-frequency sub-sequences obtained using CLSI–VMD can help to identify turning points (peaks and valleys) in the tourism market, providing better support for the decision-making of tourism managers.

This study has some limitations that can be further investigated. Firstly, during the recurrence of the COVID-19 epidemic, the forecast of tourism demand is very complicated. More predictive factors, such as the impact of policies and restrictions, may be considered. Secondly, when considering multi-source data, a more powerful predictive model is needed given the diversity and complexity of the input variables [52–54]. Finally, apart from the CLSI and VMD methods, other effective composite or decomposition methods can be employed in handling search engine data. In the future, we will further study the above-mentioned issues of tourism demand forecasting during the COVID-19 epidemic.

Acknowledgements The authors are very grateful for the constructive comments of editors and referees. This research is partially supported by the Humanities and Social Sciences Foundation of the Chinese Ministry of Education, China (No.22YJA630003).

Data availability The datasets generated during and/or analyzed during the current study are available from the corresponding author on reasonable request.

Declarations

Competing interest None.

References

1. Zhan C, Zheng Y, Zhang H, Wen Q (2021) Random-forest-bagging broad learning system with applications for COVID-19 pandemic. IEEE Internet Things J 8:15906–15918. https://doi.org/10.1109/JIOT.2021.3066575
2. Karabulut G, Bilgin MH, Demir E, Doker AC (2020) How pandemics affect tourism: international evidence. Ann Touris Res 84:102991. https://doi.org/10.1016/j.annals.2020.102991
3. Hosseini SM, Paydar MM, Hajiaghaei-Keshteli M (2021) Recovery solutions for ecotourism centers during the Covid-19 pandemic: utilizing Fuzzy DEMATEL and Fuzzy VIKOR methods. Expert Syst Appl 185:115594. https://doi.org/10.1016/j.eswa.2021.115594
4. Kim YR, Liu A (2022) Social distancing, trust and post-COVID-19 recovery. Tour Manag 88:104416. https://doi.org/10.1016/j.tourman.2021.104416
5. Wickramasinghe K, Ratnasiri S (2021) The role of disaggregated search data in improving tourism forecasts: evidence from Sri Lanka. Curr Issues Tour 24:2740–2754. https://doi.org/10.1080/13683500.2020.1849049
6. Wu DC, Cao Z, Wen L, Song H (2021) Scenario forecasting for global tourism. J Hosp Tour Res 45:28–51. https://doi.org/10.1177/1096348020919990
7. Sun S, Wei Y, Tsui K-L, Wang S (2019) Forecasting tourist arrivals with machine learning and internet search index. Tour Manag 70:1–10. https://doi.org/10.1016/j.tourman.2018.07.010
8. Li X, Li H, Pan B, Law R (2021) Machine learning in internet search query selection for tourism forecasting. J Travel Res 60:1213–1231. https://doi.org/10.1177/0047287520934871

9. Xie G, Qian Y, Wang S (2021) Forecasting Chinese cruise tourism demand with big data: an optimized machine learning approach. Tour Manag 82:104208. https://doi.org/10.1016/j.tourman.2020.104208
10. Li S, Chen T, Wang L, Ming C (2018) Effective tourist volume forecasting supported by PCA and improved BPNN using Baidu index. Tour Manag 68:116–126. https://doi.org/10.1016/j.tourman.2018.03.006
11. Peng G, Liu Y, Wang J, Gu J (2017) Analysis of the prediction capability of web search data based on the HE-TDC method aEuro' prediction of the volume of daily tourism visitors. J Syst Sci Syst Eng 26:163–182. https://doi.org/10.1007/s11518-016-5311-7
12. Varian HR (2014) Big data: new tricks for econometrics. J Econ Perspect 28:3–27. https://doi.org/10.1257/jep.28.2.3
13. Zhang H, Song H, Wen L, Liu C (2021) Forecasting tourism recovery amid COVID-19. Ann Tour Res 87:103149. https://doi.org/10.1016/j.annals.2021.103149
14. Li H, Hu M, Li G (2020) Forecasting tourism demand with multisource big data. Ann Tour Res 83:102912. https://doi.org/10.1016/j.annals.2020.102912
15. Zhan C, Jiang W, Lin F et al (2022) A decomposition-ensemble broad learning system for AQI forecasting. Neural Comput Appl. https://doi.org/10.1007/s00521-022-07448-2
16. Hassani H, Silva ES, Antonakakis N et al (2017) Forecasting accuracy evaluation of tourist arrivals. Ann Tour Res 63:112–127. https://doi.org/10.1016/j.annals.2017.01.008
17. Assaf AG, Li G, Song H, Tsionas MG (2019) Modeling and forecasting regional tourism demand using the bayesian global vector autoregressive (BGVAR) model. J Travel Res 58:383–397. https://doi.org/10.1177/0047287518759226
18. Fu Y, Hao J-X, Li X, Hsu CHC (2019) Predictive accuracy of sentiment analytics for tourism: a metalearning perspective on Chinese travel news. J Travel Res 58:666–679. https://doi.org/10.1177/0047287518772361
19. Li X, Law R (2020) Forecasting tourism demand with decomposed search cycles. J Travel Res 59:52–68. https://doi.org/10.1177/0047287518824158
20. Yao Y, Cao Y, Ding X et al (2018) A paired neural network model for tourist arrival forecasting. Expert Syst Appl 114:588–614. https://doi.org/10.1016/j.eswa.2018.08.025
21. Liang X, Wu Z (2022) Forecasting tourist arrivals using dual decomposition strategy and an improved fuzzy time series method. Neural Comput Appl. https://doi.org/10.1007/s00521-021-06671-7
22. Gao Y (2021) Forecast model of perceived demand of museum tourists based on neural network integration. Neural Comput Appl 33:625–635. https://doi.org/10.1007/s00521-020-05012-4
23. Dergiades T, Mavragani E, Pan B (2018) Google trends and tourists' arrivals: emerging biases and proposed corrections. Tour Manag 66:108–120. https://doi.org/10.1016/j.tourman.2017.10.014
24. Gunter U, Oender I (2016) Forecasting city arrivals with Google analytics. Ann Touris Res 61:199–212. https://doi.org/10.1016/j.annals.2016.10.007
25. Bangwayo-Skeete PF, Skeete RW (2015) Can Google data improve the forecasting performance of tourist arrivals? Mixed-data sampling approach. Tour Manag 46:454–464. https://doi.org/10.1016/j.tourman.2014.07.014
26. Yang X, Pan B, Evans JA, Lv B (2015) Forecasting Chinese tourist volume with search engine data. Tour Manag 46:386–397. https://doi.org/10.1016/j.tourman.2014.07.019
27. Brynjolfsson E, Geva T, Reichman S (2016) Crowd-squared: amplifying the predictive power of search trend data. MIS Q 40:941. https://doi.org/10.25300/MISQ/2016/40.4.07
28. Song H, Qiu RTR, Park J (2019) A review of research on tourism demand forecasting. Ann Touris Res 75:338–362. https://doi.org/10.1016/j.annals.2018.12.001
29. Li X, Pan B, Law R, Huang X (2017) Forecasting tourism demand with composite search index. Tour Manag 59:57–66. https://doi.org/10.1016/j.tourman.2016.07.005
30. Law R, Li G, Fong DKC, Han X (2019) Tourism demand forecasting: a deep learning approach. Ann Touris Res 75:410–423. https://doi.org/10.1016/j.annals.2019.01.014
31. Novelli M, Burgess LG, Jones A, Ritchie BW (2018) "No Ebola... still doomed"—the Ebola-induced tourism crisis. Ann Touris Res 70:76–87. https://doi.org/10.1016/j.annals.2018.03.006
32. Page S, Song H, Wu DC (2012) Assessing the impacts of the global economic crisis and swine flu on inbound tourism demand in the United Kingdom. J Travel Res 51:142–153. https://doi.org/10.1177/0047287511400754
33. Rossello J, Santana-Gallego M, Awan W (2017) Infectious disease risk and international tourism demand. Health Policy Plan 32:538–548. https://doi.org/10.1093/heapol/czw177
34. Choe Y, Wang J, Song H (2021) The impact of the Middle East Respiratory Syndrome coronavirus on inbound tourism in South Korea toward sustainable tourism. J Sustain Tour 29:1117–1133. https://doi.org/10.1080/09669582.2020.1797057
35. Shi W, Li KX (2017) Impact of unexpected events on inbound tourism demand modeling: evidence of Middle East Respiratory Syndrome outbreak in South Korea. Asia Pac J Tour Res 22:344–356. https://doi.org/10.1080/10941665.2016.1250795
36. Zeng B, Carter RW, De Lacy T (2005) Short-term perturbations and tourism effects: the case of SARS in China. Curr Issue Tour 8:306–322. https://doi.org/10.1080/13683500508668220
37. McAleer M, Huang B-W, Kuo H-I et al (2010) An econometric analysis of SARS and Avian Flu on international tourist arrivals to Asia. Environ Modell Softw 25:100–106. https://doi.org/10.1016/j.envsoft.2009.07.015
38. Gossling S, Scott D, Hall CM (2021) Pandemics, tourism and global change: a rapid assessment of COVID-19. J Sustain Tour 29:1–20. https://doi.org/10.1080/09669582.2020.1758708
39. Ying T, Wang K, Liu X et al (2021) Rethinking game consumption in tourism: a case of the 2019 novel coronavirus pneumonia outbreak in China. Tour Recreat Res 46:304–309. https://doi.org/10.1080/02508281.2020.1743048
40. Liu H, Liu W, Wang Y (2021) A study on the influencing factors of tourism demand from Mainland China To Hong Kong. J Hosp Tour Res 45:171–191. https://doi.org/10.1177/1096348020944435
41. Liu Y, Chen Y, Wu S et al (2015) Composite leading search index: a preprocessing method of internet search data for stock trends prediction. Ann Oper Res 234:77–94. https://doi.org/10.1007/s10479-014-1779-z
42. Dragomiretskiy K, Zosso D (2014) Variational mode decomposition. IEEE Trans Signal Process 62:531–544. https://doi.org/10.1109/TSP.2013.2288675
43. Liu Y, Yang C, Huang K, Gui W (2020) Non-ferrous metals price forecasting based on variational mode decomposition and LSTM network. Knowl-Based Syst 188:105006. https://doi.org/10.1016/j.knosys.2019.105006
44. Lim B, Arik SO, Loeff N, Pfister T (2021) Temporal Fusion Transformers for interpretable multi-horizon time series forecasting. Int J Forecast 37:1748–1764. https://doi.org/10.1016/j.ijforecast.2021.03.012
45. Ampountolas A (2019) Forecasting hotel demand uncertainty using time series Bayesian VAR models. Tour Econ 25:734–756. https://doi.org/10.1177/1354816618801741
46. Wu B, Wang L, Lv S-X, Zeng Y-R (2021) Effective crude oil price forecasting using new text-based and big-data-driven model.

Measurement 168:108468. https://doi.org/10.1016/j.measurement.2020.108468
47. Kulshrestha A, Krishnaswamy V, Sharma M (2020) Bayesian BILSTM approach for tourism demand forecasting. Ann Touris Res 83:102925. https://doi.org/10.1016/j.annals.2020.102925
48. Wang L, Wu B, Zhu Q, Zeng Y-R (2020) Forecasting monthly tourism demand using enhanced backpropagation neural network. Neural Process Lett 52:2607–2636. https://doi.org/10.1007/s11063-020-10363-z
49. Gundu V, Simon SP (2021) Short term solar power and temperature forecast using recurrent neural networks. Neural Process Lett 53:4407–4418. https://doi.org/10.1007/s11063-021-10606-7
50. Saab S, Fu Y, Ray A, Hauser MA (2022) Dynamically stabilized recurrent neural network. Neural Process Lett. https://doi.org/10.1007/s11063-021-10676-7
51. Geva T, Oestreicher-Singer G, Efron N, Shimshoni Y (2017) Using forum and search data for sales prediction of high-involvement projects. MIS Q 41:65. https://doi.org/10.25300/MISQ/2017/41.1.04
52. Wu B, Wang L, Zeng Y-R (2022) Interpretable wind speed prediction with multivariate time series and temporal fusion transformers. Energy 252:123990. https://doi.org/10.1016/j.energy.2022.123990
53. Wu B, Wang L, Wang S, Zeng Y-R (2021) Forecasting the US oil markets based on social media information during the COVID-19 pandemic. Energy 226:120403. https://doi.org/10.1016/j.energy.2021.120403
54. Wang L, Zeng Y-R, Zhang JL, Huang W, Bao YK (2006) The criticality of spare parts evaluating model using an artificial neural network approach. Lect Notes Comput Sci 3991:728–735. https://doi.org/10.1007/11758501_97